The far-infrared energy distributions of Seyfert and starburst galaxies in the Local Universe: ISO photometry of the 12μm active galaxy sample[1]

Luigi Spinoglio

Istituto di Fisica dello Spazio Interplanetario, CNR via Fosso del Cavaliere 100, I-00133 - Roma (Italy)

luigi@ifsi.rm.cnr.it

Paola Andreani[2]

Osservatorio Astronomico Padova, Vicolo dell'Osservatorio 5, I-35122 - Padova (Italy)

andreani@pd.astro.it

and

Matthew A. Malkan

Physics and Astronomy Department, University of California at Los Angeles, Los Angeles, CA 90095-1562 (USA)

malkan@astro.ucla.edu

ABSTRACT

New far-infrared photometry with ISOPHOT, onboard the *Infrared Space Observatory*, is presented for 58 galaxies with homogeneous published data for another 32 galaxies all belonging to the 12μm galaxy sample. In total 29 Seyfert 1's, 35 Seyfert 2's and 12 starburst galaxies, about half of the 12μm active galaxy sample, plus 14 normal galaxies for comparison. The ISO and the IRAS data are used to define color-color diagrams and spectral energy distributions (SED). Thermal dust emission at two temperatures (one cold at 15-30K and one warm at 50-70K) can fit the 60–200μm SED, with a dust emissivity law proportional to the inverse square of the wavelength. Seyfert 1's and Seyfert 2's are indistinguishable longward of 100μm, while, as already seen by IRAS, the former have

[2]Present address: Max-Planck-I. für Extraterrestrische Physik, Postfach 1312, 85741 Garching (Germany)

flatter SEDs shortward of 60μm. A mild anti-correlation is found between the [200 - 100] color and the "60μm excess". We infer that this is due to the fact that galaxies with a strong starburst component, and thus a strong 60μm flux, have a steeper far-infrared turnover. In non-Seyfert galaxies, increasing the luminosity corresponds to increasing the star formation rate, that enhances the 25 and 60μm emission. This shifts the peak emission from around 150μm in the most quiescent spirals to shorter than 60μm in the strongest starburst galaxies. To further quantify these trends, we followed Rowan-Robinson and Crawford (1989) in identifying with the IRAS colors three idealized infrared SED: that of pure quiescent disk emission, pure starburst emission, and pure Seyfert nucleus emission. Even between 100 and 200μm, the quiescent disk emission remains much cooler than the starburst component. Seyfert galaxies have 100–200μm SED ranging from pure disks to pure starbursts, with no apparent contribution from their active nuclei at those wavelengths.

Subject headings: galaxies: active – galaxies: nuclei – galaxies: photometry – galaxies: Seyfert – galaxies: starburst – infrared: galaxies.

1. INTRODUCTION

One of the main goals of selecting a complete sample of galaxies using the IRAS 12μm flux was the definition of a complete and largely unbiased sample of active galaxies in the local universe. This selection was done twice, the first one producing a list of 26 Seyfert type 1 galaxies (hereinafter Seyfert 1's) and 32 Seyfert 2's (Spinoglio & Malkan 1989), out of a sample of 390 galaxies from the IRAS PSC (1988). The second was a selection of 53 Seyfert 1's, 63 Seyfert 2's, two blazars and 38 high-luminosity non-Seyferts (i.e. galaxies with $L_{IR} \geq 10^{44}$erg s^{-1} without an obvious Seyfert type optical spectrum) out of a sample of 893 galaxies (Rush, Malkan & Spinoglio 1993) (RMS) from the IRAS Faint Source Catalog (Moshir et al. 1992). It was found that the 12μm flux is approximately a constant fraction ($\sim 1/5$) of the bolometric flux in active galaxies. Moreover, also for non-Seyferts (mostly spirals) 12μm selection was found to be the closest available approximation to selection by a limiting bolometric flux, which is about 14 times $\nu\ F_\nu$ at 12μm (Spinoglio et al. 1995)

[1]Based on observations with ISO, an ESA project with instruments funded by ESA Member States (especially the PI countries: France, Germany, the Netherlands and the United Kingdom) with the participation of ISAS and NASA

(hereinafter S95). It therefore follows that deep surveys at $12\mu m$ should provide complete samples at different bolometric flux levels of normal and active galaxies, which will not suffer the strong selection effects present both in the optical-UV and far-infrared. We refer to the introduction of the paper presenting the original sample (Spinoglio & Malkan 1989) for the arguments in favor of the mid-infrared selection. After the determination by RMS, two more works derived the local $12\mu m$ luminosity function (Xu et al. 1998; Fang et al. 1998) and a new selection of galaxies from the IRAS database at $12\mu m$ is in progress (Alexander & Aussel 1999).

The study of the infrared energy distributions of active and starburst galaxies in the local universe is not only important by itself, but also because it is needed to understand galaxy evolution. Deep ISO surveys have shown that indeed a strong evolution is present at $z \sim 1$, indicating that many galaxies at that epoch were experiencing phases of extremely high luminosities in the far-infrared, likely to represent violent events of star formation [see e.g. the reviews of Malkan (2000), Genzel & Cesarsky (2000), and Franceschini et al. (2001)]. Also, the peak of the energy output of galaxies lies in the far-infrared. This makes redshifted galaxies appear relatively brighter at the longest far-infrared and sub-millimeter wavelengths; surveys in these wavebands are therefore capable of discovering very distant galaxies at substantial cosmic look-back times (see e.g. Malkan 2001). It is thus even more urgent to understand the local infrared emission, to provide a firm base for comparing the local universe "activity" with the properties and evolution observed in the recent and upcoming cosmological surveys (e.g. Franceschini et al. 2001; Malkan 2001).

Several papers have reported ISO photometric data on galaxies in the unexplored range from 100-200μm, but most of these are on few individual sources, often the prototypes of the various classes of active, starburst and normal galaxies. The only exceptions are the study of 42 objects (20 Seyfert 1's and 22 Seyfert 2's) (Pérez García & Rodríguez Espinosa 2000)(PGRE) of the CfA Seyfert galaxy sample (Huchra & Burg 1992), the study of a random sample (Haas et al. 2000) of 17 Palomar Green quasars (Schmidt & Green 1983), the study of 22 radio-loud and radio-quiet quasars (Polletta et al. 2000) and one of 10 galaxy/quasar pairs from the 3CR catalog (Meisenheimer et al. 2001). The CfA Seyfert galaxy sample is smaller (48 objects) than the $12\mu m$ active galaxy sample (158 objects), and is selected by the optical light of the galaxy, which may bias the results significantly. For example, a recent work on high resolution radio observations of the Seyfert galaxies of the $12\mu m$ sample (Thean et al. 2000, 2001), report a detailed statistical analysis of the redshift distributions and $12\mu m$ flux distributions of Seyfert 1's and 2's and compared these with the CfA sample. In the $12\mu m$ active galaxy sample the two types of Seyferts are equally distributed according to redshift, their $12\mu m$ flux density distributions are well matched and therefore Seyfert 1's and 2's are equally luminous in the IRAS $12\mu m$ band. On the contrary, the CfA Seyfert

sample has different redshift distributions for the two Seyfert types, and is biased against including distant Seyfert 2's.

The three latter works on quasars (Haas et al. 2000; Polletta et al. 2000; Meisenheimer et al. 2001) are complementary to ours since most of the sources have much higher redshifts ($0.1 < z < 2.0$). However, these studies are not suited to studying the population of active galaxies in the local universe.

The present work is based on observations of 90 galaxies, randomly selected from the $12\mu m$ galaxy sample, including 29 Seyfert 1's, 35 Seyfert 2's, 12 high luminosity non-Seyferts (hereafter called starburst galaxies) and 14 normal galaxies for comparison. It is the largest sample of active galaxies for which far-infrared photometry is available out to $200\mu m$. Since it contains both active and starburst galaxies it is expected to be the basis for firm and statistically significant conclusions on the far-infrared behaviour of galaxies in the local universe.

The paper is organized as follows: section 2 describes the observations collected and reduced longward of $100\mu m$; section 3 shows the results in terms of average energy distributions and presents a derivation of "pure" infrared emission components, for quiescent disks, starbursts, and Seyfert nuclei; section 4 shows the color-color diagrams of the various classes of galaxies that can be explained by thermal emission from dust and presents a correlation between the far infrared color [200 - 100] and the $60\mu m$ excess; section 5 shows the correlations among the different luminosities and between colors and luminosities. Section 6 presents our conclusions. Finally, in the Appendix we present the results obtained shortward of $100\mu m$.

2. OBSERVATIONS

The Infrared Space Observatory (ISO) (Kessler et al. 1996) data presented here were obtained in the open time proposal "IR energy distributions and imaging of the complete sample of $12\mu m$ active galaxies". Photometric data at several wavelengths between 60 and 200 μm were collected with the two array cameras, C100 and C200 of the ISOPHOT imaging photo-polarimeter (Lemke et al. 1996). In particular, we present in this section the ISOPHOT photometric results obtained with the C200 detector array in the spectral range 120-$200\mu m$ on 39 objects belonging to the $12\mu m$ active galaxies sample. The data obtained with the C100 array camera are presented in Appendix 1, for two reasons: first, these data are less precise than the C200 data, having larger uncertainties, due either to a difficult subtraction of the background and to a less accurate calibration (see the discussion in Appendix 1);

second, these data are less important, because all the galaxies of the sample have good IRAS detections at 12, 25, 60 and 100μm. To increase the statistics, we have also analyzed ISOPHOT C200 archive data on other 19 galaxies and we have included in the discussion ISOPHOT literature data on another 32 galaxies, bringing the present sample to 90 objects. This is therefore currently the largest sample of active galaxies in the local universe studied to 200μm.

The journal of the C200 ISOPHOT observations is given in Table 1, which presents the details of each single observation that we analysed: for each source are given the coordinates of the observations, the redshift, the galaxy type (hereafter we call starburst nuclei *sbn* the high luminosity non Seyfert galaxies), the ISO observation identification number and the total integration time spent on-source.

All of the detections are consistent with that expected for unresolved point sources. That is, none of the galaxies were significantly resolved by the large ISOPHOT PSF, which is estimated to be $\sim 100\,''$ FWHM in diameter at 120 μm [e.g. see Fig.4.8 of Laureijs et al. (2001)].

The C200 ISOPHOT observations were collected in chopped photometric mode in the five filters centered at 120, 150, 170, 180 and 200μm. The data reduction has been performed using the PIA[3] software, version 7.2 (Gabriel et al. 1997) and the results were verified with version 8.0. Data were deglitched, corrected for non-linearity and then for each ramp a straight line was fitted. In most cases the first signal per chopper plateau was discarded since the detector response was not stabilized. Then the data were corrected for dark current and for signal dependence on the ramp integration time and calibrated with the internal Fine Calibration Source (FCS1). The same reduction procedure was applied also to the calibration data. An independent reduction of several of these observations was made by one of us (MM) at IPAC[4], those results are in good agreement with the values published here. We realize there are faint outer parts to some of these galaxies, and this was even measured and discussed in the appendix of RMS. However, we find that only a small fraction of the total flux is actually missed due to the central concentration of the light, and that our colors should be very reliable anyway, one of the main points of this study.

The ISOPHOT flux densities have been corrected using the color correction, from the PIA (Gabriel et al. 1997), corresponding to black-body functions with an emissivity law

[3]PIA is a joint development by the ESA Astrophysics Division and the ISOPHOT consortium led by the MPI fur Astronomie, Heidelberg. Contributing institutes are DIAS, RAL, AIP, MPIK and MPIA.

[4]IPAC (Infrared Processing and Analysis Center) is part of the Division of Physics, Mathematics and Astronomy at Caltech, Pasadena, and the Space and Earth Sciences Program Directorate at JPL, Pasadena.

proportional to the inverse square of the wavelength. The chosen dust temperatures were the lowest color temperature that we derive from the [200 - 100] color of each class of galaxies, derived from the positions in the far-infrared color-color diagrams presented in section 4. They are 20K for Seyfert 1's and normal galaxies, 25K for Seyfert 2's and 30K for high luminosity non-Seyferts. At these temperatures, the color correction is, however, quite small (less than 15%).

Because all the galaxies have good detections in all the IRAS bands, we have constructed their spectral energy distributions using the new ISOPHOT data together with the IRAS data given in RMS. In Fig. 1 we present the spectral energy distributions of each individual object. Table 2 presents the measured flux densities and 1 σ statistical errors in the five ISOPHOT C200 wavebands for each object. Absolute calibration uncertainty is in the range 10—30%.

For most of the sources a good general agreement is found between IRAS and ISO measurements and the C200 values place themselves on a smooth curve running from the IRAS to the ISO photometry. Data for Arp 220, NGC 6240 and IZW 1 were taken from the archive. The results reported here agree well with those published in the literature for the first two sources (Klaas et al. 1997) while the C200 data of IZW 1 of Table 2 agree with those published by Haas et al. (2000) but not with those by PGRE. The measurements were taken with different observational setups, the ones reported here were gathered in chopping mode while those by PGRE in staring mode and the resulting values are much lower in this latter case. We ascribe this difference to the different background subtraction procedure and it could be due to an overestimation of the background value by this latter authors. They indeed did not detect IZw 1 at 200μm while we obtained a signal-to-noise ratio larger than 18 at the same wavelength. Data taken towards NGC 6090 (MK 496) reported here are lower than those published by Calzetti et al. (2000) by a factor of 1.3-1.7, however they agree within the large errors quoted by these authors.

In the following analysis we also included the ISO results published by several authors on galaxies belonging to the 12μm galaxy sample: 17 CfA Seyfert galaxies (PGRE), 10 normal galaxies (Siebenmorgen, Krugel & Chini 1999), 4 nearby spiral galaxies (Alton et al. 1998) and the Seyfert 2 NGC 7582 (Radovich et al. 1999). The CfA Seyfert 1's included are: NGC 3227, NGC 3516, NGC 4051, NGC 4151, MK 766, MK 231, NGC 5033, NGC 5548, MK 817 and NGC 7469, while the CfA Seyfert 2's are: NGC 1143/44, NGC 3079, NGC 3982, NGC 4388, NGC 5256, NGC 5929 and NGC 1068. The normal galaxies included are: MK 323, MK 332, MK 555, MK 538, MK 799, NGC 5719, NGC 6918, NGC 7083, UGC 2936 and UGC 2982 and the nearby spiral galaxies are: NGC 134, NGC 660, NGC 5194 and NGC 5236.

Table 3 gives the integrated mid-to-far infrared luminosity from 8 to 250μm for all 90 galaxies, including those taken from the literature. This luminosity has been computed using the formula:

$$L_{FIR} = 4\pi(\frac{cz}{H_o})^2 \times \sum_i (S_{\nu_i} \times \Delta\nu_i) \times 10^{-11} \mathrm{erg\ s^{-1} cm^{-2}} \quad (1)$$

with the S_{ν_i} the flux densities in Jy and $\Delta\nu_i$ = 13.48, 5.16, 2.58, 1.0, 1.04, 1.02, 0.95, 0.65, 0.48, for λ_i = 12, 25, 60, 100, 120, 150, 170, 180 and 200 μm, respectively[5]. We adopted a value of H_o = 75 km s^{-1} Mpc^{-1}.

To show how the present sub-sample is representative of the 12μm active galaxy sample, we have computed average redshift and completeness of the sub-sample and compared with that of the original sample (RMS). The average redshift of the Seyfert 1's in the present sub-sample is $\langle z \rangle = .029 \pm .034$, compared to the value of $\langle z \rangle = .030 \pm .038$ of the original sample; that of the Seyfert 2's is $\langle z \rangle = .021 \pm .018$, which is exactly the same of the value of the original sample; that of the starburst galaxies is $\langle z \rangle = .034 \pm .014$, compared to the value of $\langle z \rangle = .030 \pm .010$ of the original sample. The completeness test was applied only to the Seyfert galaxies, because the starburt nuclei of the 12μm sample are not supposed to be a complete sample (see RMS): the present sub-sample contains 63% of the Seyfert 1's and 57% of the Seyfert 2's of the original sample down to a flux limit of 0.30 Jy at 12μm and 61% of the Seyfert 1's and 64% of the Seyfert 2's of the original sample down to 0.40 Jy. We conclude from this analysis that the present sub-sample represents fairly well the 12μm active galaxy sample, and there is no apparent bias.

3. SPECTRAL ENERGY DISTRIBUTIONS

3.1. Average energy distributions

Fig. 2 shows the average observed power $\nu \times F_\nu$ from 4400 Å to 200μm of each class of galaxies (except for the very few nearby spiral galaxies, for which the statistics is poor) normalized to the 12μm power observed by IRAS. The optical and near-infrared data have been corrected for aperture sizes to represent the total fluxes (S95). The shape of the optical-to-far-infrared spectral energy distribution (hereinafter SED) changes from one class

[5]The four frequency intervals ($\Delta\nu_i$) relative to the IRAS wave-bands have been taken from Rowan-Robinson and Crawford (1989), while the others have been computed from Table 2.7 of Laureijs et al. (2001).

to another: Seyfert 1's show a general decrease from the optical to the far-infrared with only a small bump around the L ($3.6\mu m$) band; Seyfert 2's show two pronounced peaks with about the same power around the J-H bands (1.2-1.6μm) and at $60\mu m$; starburst galaxies have again the same two peaks in their SEDs, but the far-infrared peak is much brighter than the near-infrared peak; finally normal galaxies show two peaks with about the same power.

To better show the far-infrared turnover, we show in Fig. 3 the mean far-infrared SED for each class of galaxies, except nearby spirals, normalized to the observed power at $60\mu m$.

The main results here are: *i)* Seyfert 1's have a flatter SED shortward of $60\mu m$, compared to all other classes of galaxies; *ii)* the two Seyfert types have virtually identical spectra from 60 to $200\mu m$, while they appear different only shortward of $60\mu m$; *iii)* the SED of starburst galaxies show the steepest drop off beyond $60\mu m$; *iv)* the normal galaxies in the sample observed show stronger emission at wavelengths longer than $150\mu m$ than the other types of galaxies.

The various types of galaxies show a sequence in the slope of the short wavelength part of the SED (from 12 to $60\mu m$) from the very flat Seyfert 1's, through the intermediate Seyfert 2's, to the steep starburst and normal galaxies. The flatter SED of Seyfert 1's in the range 12-120μm probably arises from the warmer dust heated by the active nucleus.

3.2. Testing unified models of Seyfert 1's and 2's

Unified models claim that the observational differences between Seyfert 1's and 2's can be attributed to the different orientation of a hypothetical dusty torus (e.g. Antonucci 1993). To test this hypothesis, we have fitted in Figure 4 the average slope of the 12-200μm far-infrared SEDs of Seyfert 1's and Seyfert 2's with the sum of an optically thick dusty torus seen face and edge on respectively, from the models by Granato & Danese (1994) and grey-body thermal emission at 25K with inverse square wavelength dependence of the dust emissivity (meant to represent the extended dust emission from the galactic disk). As shown in Figure 4, the cool component produces about 40% of the observed fluxes at 60μm. Although any detailed model fitting is beyond the scope of the present paper, there is a rough qualitative consistency between the data and this simple model. However, *in detail the model fails* because it does not predict strong enough flux *differences* at 12 and 25μm as the torus orientation shifts from face-on to edge-on. With a more realistic *range of torus orientations* in Seyfert 1's and 2's, the disagreement with observations would be even more significant.

3.3. Spectral Decomposition of Active and Quiescent Components

In this section we investigate if the decomposition of the observed SEDs in physically distinct spectral components that was proposed by Rowan-Robinson and Crawford (1989) (RRC) for the IRAS data can be extended to the longer wavelength ISO results.

First, we discuss the SED as defined by the IRAS data only: if we simply take the average flux ratios among the four IRAS wavelengths ($F_{12\mu m}$: $F_{25\mu m}$: $F_{60\mu m}$: $F_{100\mu m}$) of the different types of galaxies, from our sample we obtain for Seyfert 1's: 1 : 2.3 : 10.3 : 21.7, for Seyfert 2's: 1 : 3.3 : 20 : 29.2, for starburst galaxies: 1 : 4.5 : 27 : 35 and for normal spiral galaxies: 1 : 2.4 : 16 : 30. Subtracting the normal galaxies ratios from those of starburst galaxies, we are able to identify a "warm" starburst component with ratios: 1 : 2 : 11 : 5, peaking at 60μm. As an exercise, if we add together the ratios of Seyfert 1's with those of this warm starburst component, we can roughly reproduce the ratios of Seyfert 2's. This suggests that there might be a difference between the two types of Seyfert nuclei in the star forming activity of their host galaxies, confirming the finding that Seyfert 2 nuclei lie preferentially in galaxies experiencing more enhanced star forming activity compared to Seyfert 1's (Maiolino et al. 1995). It is possible that this results from a selection effect: since Seyfert 2 nuclei are relatively weaker at $12\mu m$ than Seyfert 1's, they are more likely to fall into our flux-limited sample if their brightness at this wavelength is enhanced by strong star formation.

We want now to extend the analysis including the longer wavelength ISOPHOT data. Our broad-band SEDs are probably too crude a description of the complexities of galaxies to allow a full principal component decomposition into physically distinct emission components. Nonetheless, we have followed RRC in using the 12-25-60-100μm colors to identify those galaxies in our sample which closely resemble the SEDs of the "quiescent cirrus" disk, the "starburst" component, and the "pure Seyfert" nucleus. For each of the three types of galaxies, the normal spirals, the starburst galaxies and the Seyfert 1's, we have selected those objects lying in the two IRAS color-color diagrams close (i.e., within 0.2 magnitudes) to the colors of "pure disc", "starburst" and "Seyfert" components of RRC (labeled D, B and S, respectively in Fig.1 of RRC). We have then plotted in Fig.5 the complete 12-200μm SEDs of the selected galaxies individually and their average value for each class in Fig.6.

As shown in Fig.5, five normal spiral galaxies have nearly the RRC colors of the "pure cirrus disk" component: $F_{12\mu m}$: $F_{25\mu m}$: $F_{60\mu m}$: $F_{100\mu m}$ = 1:1:12.7:40. These are the only normal galaxies in our sample that have the color [60 - 25]$\geq$0.8 and the color [100 - 60]$\geq$0.3. Similarly seven starburst galaxies have IRAS colors close to the "pure starburst" spectrum with the four IRAS fluxes scaling as 1:5:24.5:24.5. These galaxies have been selected because they are the only starburst galaxies in our sample with 0.6$\leq$[60 - 25]$\leq$0.9 and -0.05$\leq$[100 - 60]$\leq$0.25. Seven Seyfert 1's galaxies have IRAS colors near the "pure Seyfert nucleus" and are

the only Seyfert 1's in our sample with [60 - 25]≤0.25 and [25 - 12]≥0. As also confirmed from our discussion of the two colors diagrams (see subsection 4.1), the strong distinction between quiescent disks and starbursts remains clear out to 200μm. The cirrus and starburst spectra probably represent extremes of minimal and maximal recent star formation, that tend to be found in the least and most luminous galaxies, respectively. The pure Seyfert spectrum is rather similar to the pure starburst spectrum between 100 and 200μm. Both show a relative lack of cold dust, and the Seyfert's tend to be weaker at 120μm.

The Seyfert 2's are spread all around the IRAS color-color diagrams. As can be seen in Fig.5, some of them have IRAS spectra close to the pure starburst template (we have selected four in Fig.5). And indeed their ISOPHOT far-infrared spectra also match the pure starburst spectrum well, since their infrared continuum appears to be dominated from dust around star forming regions. Those Seyfert 2's with IRAS colors like quiescent cirrus disks also resemble pure disks in the 100–200μm region. Again it appears that the Seyfert 2's nucleus contributes a minor fraction of the observed far-infrared luminosity in those objects.

4. COLOR-COLOR ANALYSIS

4.1. Far-infrared color-color diagrams

We have constructed color-color diagrams with the ISO and IRAS photometry to see how the SEDs of the different classes of galaxies differ, and if these can be used to segregate them. Fig.7 and 8 show, respectively, the [200 - 100] versus [60 - 25] and the [200 - 100] versus [100 - 60] color-color diagrams[6]. The averaged colors for each type of galaxies are reported in Table 4.

From the two diagrams we conclude:

1. For non-Seyfert galaxies, our interpretation of the different positions of the different types of galaxies in Fig.8 is that the [100 - 60] and especially the [200 - 100] colors define a correlated sequence running from galaxies with the weakest star formation up to the starbursts, in agreement with the SED behaviour as shown in Fig.3; Table 4 can be used to quantify this result: the [100 - 60] colors of starburst and nearby spiral galaxies do not overlap each other at the 1σ level; even better, the [200 - 100] color is

[6]We define color

$$[\lambda_1 - \lambda_2] = Log(F_\nu(\lambda_1)/F_\nu(\lambda_2))$$

where $F_\nu(\lambda_i)$ is the flux density in Jy at λ_i.

able to separate starburst from normal and normal from nearby spiral galaxies, while the colors of Seyfert's are intermediate between starburst and normal galaxies.

2. The star formation rate does not, however, influence the [60 - 25] colors; from Table 4 we note that the [60 - 25] color is virtually the same among starburst, normal and nearby spiral galaxies. The [60 - 25] color only shows a small displacement between Seyfert 1's and 2's, and Seyfert galaxies in general from normal and starburst galaxies; its average value decreases moving to Seyfert galaxies and becomes the lowest for Seyfert 1's (Table 4). However, as can be seen from the Table 4, the scatter in individual galaxies is comparable to the amount of this weak shift, making it marginally significant.

3. Seyfert 1's and 2's are not distinguishable from normal galaxies, or from each other in either [100 - 60] or [200 - 100] colors; as Table 4 shows, for both colors Seyfert and normal galaxies overlap at the 1σ level.

4. As can be seen from both Fig. 7 and 8 and from Table 4, all the infrared colors of the CfA Seyfert's are more similar to those of normal inactive galaxies than are those of our 12μm Seyfert's.

The first result indicates that both [200 - 100] and [100 - 60] colors decrease when star formation activity increases. We will confirm (see subsection 4.4) that the former color also correlates with the 60μm excess, that we consider a measure of the star formation activity in a galaxy. The second result was already known (e.g. S95). It comes about because recent star formation boosts both the 25 and 60μm luminosities of galaxies in the same proportions found in quiescent spiral galaxies. The ratio of these two luminosities remains constant. The best explanation for the third result is that none of the Seyfert nuclei in these galaxies make a substantial contribution to the total fluxes observed at wavelengths of 60μm and longward. The emission from Seyfert nuclei is relatively stronger at 25μm, compared with that of normal galactic disks. This indicates that the thermally emitting dust in Seyfert nuclei has a substantially hotter temperature distribution than in normal galaxies, even those with strong starbursts. Furthermore, the dust temperatures in Seyfert 1's tend to be even higher than those in Seyfert 2's, as was already appreciated by Edelson & Malkan (1986) and Edelson, Malkan & Rieke (1987). The fourth empirical result illustrates a general difference between the CfA and our 12μm Seyfert samples: in the former the active nuclei tend to be relatively less luminous than their host galaxies. This results in far-infrared colors in the CfA Seyfert's which are more "normal", i.e. similar to those of non-active spiral galaxies. One prediction is that the mid-infrared (10–25μm) "compactness" [defined in Edelson & Malkan (1986) as the ratio between the flux in a small beam and the total integrated flux] of the CfA Seyfert's is less than that of the 12μm Seyfert's, even at a given redshift.

Figures 9 and 10 show the far-infrared colors [150 - 100] and [200 - 150] versus the IRAS colors [60 - 25] and [100 - 60], respectively. The [200 - 150] color is able to separate starburst from normal galaxies, as is the [200 - 100] color, while the [150 - 100] color is not. This means that the separation in mainly due

to the longer wavelength slope. Finally the separation between CfA and non-CfA Seyfert galaxies is even more apparent in the [200 - 150] color than in the [200 - 100] color. The CfA Seyfert's lie in the upper part of the diagrams at [200 - 150] > -0.4, towards the position of normal galaxies, while most of the non-CfA Seyfert's are located at [200 - 150] < -0.4.

4.2. Spectral Curvature

Color-color diagrams can also be used to understand if the spectra between 100–150 and 150–200 μm can or cannot be described by simple power laws. In Fig. 11 we compare the 120 to 100μm flux ratio with the broader wavelength baseline of 100 to 150μm. The solid line shows the values that would be observed for pure power laws $F_\nu \propto \nu^\alpha$ with:

$$\alpha = \frac{log(F_{\nu_1}/F_{\nu_2})}{log(\nu_1/\nu_2)} = \frac{log(F_{\nu_1}/F_{\nu_3})}{log(\nu_1/\nu_3)} \tag{2}$$

where ν_1, ν_2 and ν_3 are three generic frequencies and F_{ν_i} the correspondent flux densities.

However, most galaxy flux ratios are better fitted with curved 100–120–150μm spectra. Points lying to the right of this line show downward spectral curvature. Most of the sample — except for 4 normal galaxies and a few low-luminosity Seyfert's — do in fact have stronger 120μm emission than would be predicted by a power-law interpolation between 100 and 150μm. Relative to their 100 and 150μm fluxes, only a few galaxies show deficits of 120μm emission. The dashed regression line (Fig.11),

$$[150 - 100] = 1.06 \times [120 - 100] - 0.09 \tag{3}$$

shows relatively little scatter about it. The dispersion of 0.09 dex corresponds to random errors in each flux of 16%, not much larger than our typical uncertainties. The line correspondent to pure power law behaviour for these colors has a slope of 2.22 compared to the flatter slope of 1.06 fitting the data.

Similarly, the regression line fitting the [170 - 150] color versus the [200 - 150] color is given by:

$$[170 - 150] = 0.09 \times [200 - 150] - 0.03 \quad (4)$$

The line correspondent to a pure power law for these two latter colors has a slope of 0.43 compared to the flatter slope of 0.09 fitting the data.

The situation appears even simpler for the 180μm flux, which generally does fall near a power law interpolation between 150 and 200μm (as shown by the solid line in Fig. 12). Thus we find that for most galaxies, measurements of 100, 150 and 200μm would be sufficient to predict the 120, 170 and 180μm fluxes accurately, but not with a simple power law interpolation.

4.3. Dust Color Temperatures

Another important outcome that can be derived from the color-color diagrams is the estimate of the temperature(s) that is (are) dominating the emission in the far-infrared. To perform this analysis we have chosen the [200 - 100] versus [60 - 25] color-color diagram and we adopted for fitting the combination of two grey-bodies, leaving to vary the dust emissivity law. We show this color-color diagram separately for the different types of galaxies in Fig. 13. The emission is broad-band: fitting it from 25 to 200μm requires a range of dust temperatures. To compare the model with the observed colors, we have overplotted the combination of the two grey-bodies in Fig. 13. This introduces the minimum necessary number of fitting parameters. To fit the long-wavelength color a steep dependence of the dust emissivity law is needed,

$$\epsilon(\lambda) \times B(\lambda, T) \quad \text{with} \quad \epsilon \propto \lambda^{-2} \quad (5)$$

A much flatter wavelength dependence would not fit most of the 200μm data for any type of galaxies.

The non-Seyfert galaxies show a clear sequence of increasing average dust temperature going from the nearest spirals up to the most luminous starbursts. The correlation of the two colors is:

$$[200 - 100] = 1.125 \times [60 - 25] - 1.252 \quad (6)$$

(the linear regression coefficient is 0.33 for 25 data points) or alternately, for the [100 - 60] color:

$$[200 - 100] = 1.626 \times [100 - 60] - 0.700 \quad (7)$$

(the linear regression coefficient is 0.73 for 26 data points)

These correlations are essentially re-statements of the correlation first presented by S95, in their Appendix B (see their Figure 13). The corresponding shift in grey-body temperature that we find is the same as what they found, after correction for the fact that their shallower wavelength dependence of dust emissivity made their fitted temperatures systematically higher than ours for a given observed spectrum. Our interpretation is that higher rates of star formation raise the average dust temperature, shifting the peak of the thermal dust emission to higher frequencies, and tilting the entire far-infrared spectrum toward the blue. Splitting the 100–200μm spectrum into two pieces, we find that most of this curvature occurs between 150 and 200μm.

In the normal spirals belonging to the $12\mu m$ galaxy sample and observed by Siebenmorgen, Krugel & Chini (1999) and by Alton et al. (1998), dust at even lower temperature (15 K) is detected, confirming the previous finding of these latter authors.

Most of the Seyfert 1's far-infrared data occupy a region that can be fitted by the mixture of two grey-bodies with $T_{min} = 22$K and $T_{max} = 55 - 70$K. The three nearby CfA Seyfert 1's galaxies (NGC 3227, NGC 5033, NGC 4051, with data taken from PGRE) with an average redshift of z=0.0031, show the highest value of the [200 - 100] color, requiring a lower minimum dust temperature (the fit in Fig. 13a gives $T_{min} = 18$K).

Almost all Seyfert 2's far-infrared data (Fig. 13b) can be fitted by the mixture of two grey-bodies with $T_{min} = 25$K and $T_{max} = 55 - 65$K. They show a somewhat narrower temperature distribution compared to Seyfert 1's, and do not extend to the higher values. Again the four reddest CfA Seyfert 2's — NGC 4388, NGC 3982, NGC 1143/44 and NGC 3079 — (PGRE) with the coolest dust ($T_{min} = 20$K), have an average redshift of 0.011, as opposed to 0.019 for all the other Seyfert 2's plotted.

Comparing the three classes of galaxies, there is a trend with the most active objects (Seyfert 1's) have the widest temperature range (22–70K); Seyfert 2's are intermediate, while starbursts have the warmest low temperature component (30K), together with the coldest high temperature one (60K).

A similar result has been found by Klaas et al. (1997) analyzing the ISOPHOT data of the three interacting galaxies Arp 244, NGC 6240 and Arp 220: the increase of the highest dust temperature component is accompanied by the decrease of the lowest dust temperature component they detect. In four narrow-line Seyfert 1's Polletta & Courvoisier (1999) found

that the lowest dust temperature is in the range 20-40K.

We are aware that there could be an additional selection effect in nearby galaxies if there is very extended emission from the galaxy discs. Measurements not performed in mapping mode could have lost some of the long wavelength emission. The detection of very cold dust only in nearby objects could thus be explained with the very low surface brightness of its thermal emission. This dust component has been found by Alton et al. (1998) to be surprisingly extended. We cannot exclude therefore that also for our objects there might be emission from cold dust (T $\sim$ 15K) that escaped detection with our observations.

4.4. The far-infrared turnover versus the 60μm excess

In this subsection we want to relate the strength of the star formation activity in a galaxy with the steepness of the far-infrared turnover, measured by the [200 - 100] color, with the aim to see how the different classes of galaxies behave and if there is a separation between galaxies with and without active nuclei.

We have chosen as the indicator of enhanced recent star formation, which warms dust around HII regions, the 60μm "excess" as the ratio of the observed 60μm flux to the flux that a source would have at 60μm from power-law interpolation of the flux between 12 and 100μm. We have already seen (see subsection 4.1) that the starburst galaxies of our sample are characterized by a low value of their [200 - 100] color. In Fig.14 we plot the [200 - 100] color index as a function of the 60μm excess. We find a correlation between the steepness of the far-infrared (100–200μm) turnover and the strength of the 60μm "excess". While this diagram does not perfectly separate the galaxies of different classes, it nevertheless shows that they cluster preferentially in different regions of the diagram. Seyfert 1's (excluding six objects of the CfA sample) cluster in a no-60μm excess region with a color [200 - 100] < 0. The starburst galaxies cluster in the central area of the diagram and have all 60μm excess. Normal galaxies and nearby spirals have no 60μm excess (except 2 objects) and a color $-0.5 < [200 - 100] < +0.5$. Seyfert 2's are widely spread all over the diagram, but with a 60μm excess generally higher than Seyfert 1's. Four especially infrared-luminous galaxies — MK 273, Arp 220, MK 938 and FSC05189-2524 lie in the "starburst" zone. In fact detailed mid-infrared spectroscopy (in the range 3-30μm) suggests that much of the total infrared luminosity in these extreme objects is indeed powered by star formation (Genzel et al. 1998). As we already noted, many of the CfA Seyfert galaxies have higher excess and/or higher [200 - 100] color, with respect to the other Seyfert galaxies. This is presumably because their faint Seyfert nuclei are too feeble to influence the overall far-infrared continuum emitted by their bright host galactic disks.

As stated above, the 60μm excess is measured with respect to the underlying 12 and 100μm fluxes, which are dominated by the "cirrus" component powered by the integrated stellar luminosity in the galaxy. When the 60μm bump is especially strong, the warm dust associated with recent star formation even contributes to the observed 100μm flux, making a relative excess at that wavelength compared with the emission from cold dust at longer wavelengths. The result is that the more actively star-forming galaxies, such as infrared-luminous starbursts, have the sharpest far-infrared turnover. They show the *steepest* drop off from 100 to 200μm, with an average slope over that wavelength range of $\alpha_{100-200\mu m} = +$ 2.2, compared to $\alpha_{100-200\mu m} = +$ 1.4, $\alpha_{100-200\mu m} = +$ 1.6 and $\alpha_{100-200\mu m} = +$ 0.8 for Seyfert 1's, 2's and normal galaxies, respectively (see Table 4).

A simple least squares fit to the data show a correlation of the color [200 - 100] with the 60μm excess with a linear regression coefficient of R=-0.48 (for 83 objects), corresponding to a probability of 99.9996%. This correlation improves by excluding the Seyfert 1's (R=-0.61 for 65 objects).

We suggest that that the diagram shown in Fig.14 can be used to separate the *starburst dominated* objects from the *AGN dominated* ones. Objects located in the upper right part of the diagram are "more" starburst dominated, while those at the left, having a fainter excess, are the AGN dominated objects. We suggest that starburst activity in galaxies, i.e. with high rates of current star formation, results in excess emission in the 60μm band accompanied by a general heating of the galactic ISM and thus a decrease of the [200 - 100] color.

We note that many of the Seyfert galaxies of the CfA sample are shifted upwards in Figure 14 with respect to the bulk of the 12μm Seyfert's. Again we interpret this as an indication that their stronger long-wavelength emission arises from the dominance of quiescent disk dust.

5. LUMINOSITY ANALYSIS

5.1. Luminosity Correlations

In this subsection we analyze the correlations of the 200μm luminosity with the luminosity in each of the IRAS bands and the total mid- to far-infrared luminosity. Although diagrams which correlate one luminosity with another in the same object should be used with caution, we have a large sample with good selection criteria in which the luminosities span over 4 orders of magnitude. In Figures 15 and 16 we show such correlations and give the formulae for the best-fitting regression lines. As expected, the slopes in the correlations of

the 200μm luminosity against the 25 and 60μm luminosities are flatter than those against the 12 and 100μm luminosities (see also S95). This is because the 25 and 60μm luminosities are preferentially elevated in those galaxies with more active recent star formation. The 100μm and 200μm emission, in contrast, are relatively stronger in the quiescent disk emission (see below), and correlate almost linearly with each other.

These figures are a logical extension of the findings of S95. They showed that galaxies with higher bolometric luminosity are relatively brighter in the 25 and 60μm bands, due to the elevated "starburst" component in them, while they appear relatively fainter at both shorter (12μm) and longer (100μm) wavelengths. The "pivot points" at which the relative luminosity neither increases nor decreases, occur around 12 and 100μm. This is our interpretation of why the 12 and 100μm luminosities have a correlation with the bolometric luminosity with a flatter slope (1.06 and 1.13, respectively) compared to the slope of the correlations of the 25 and 60μm luminosities with the bolometric luminosity ($\sim$ 1.2)(see Fig.7 of S95). For wavelengths much shorter than 12μm or longer than 100μm we therefore expect the luminosity to track less than linearly with the bolometric luminosity. That is what these figures are showing.

It is not particularly surprising that the 200μm luminosity correlates most closely with the 100μm luminosity, given that these are the two closest wavelengths. The fact that the Seyfert galaxies (of both types 1 and 2) lie on the same track as the non-Seyfert's once again indicates that the Seyfert nucleus makes a negligible contribution at these wavelengths. Since the 200μm luminosity is dominated by the "quiescent cirrus" component, it does not increase as fast as the 25 or 60μm luminosities, which are strongly effected by starbursts. Thus the slopes of the correlation between the 200μm luminosity and those at these latter wavelengths are much flatter than 1 (0.83 and 0.86 respectively).

The 200μm luminosity even decreases less rapidly than the total luminosity. This is seen by the flat slope of only 0.79 in Figure 16, where the X-axis is the "total" mid- to far-infrared luminosity, defined in equation (1) and given in Table 3. We note that a similar slope (0.87) is relating the optical blue luminosity with the bolometric luminosity (see Fig.10 of SM95), confirming the above interpretation.

5.2. Color-luminosity diagrams

As discussed above, it is believed that the more luminous non-Seyfert galaxies have higher light/mass ratios. They are luminous not so much because they are bigger or more massive, but principally because they have higher proportions of recently formed stars, which

are highly luminous. A higher proportion of their total luminosity emerges in the far-infrared, and in particular from the warmed dust grains which emit strongly at 25–60μm–what we describe as the "starburst" component (e.g. S95). One consequence of this is that the most actively star-forming galaxies should have the sharpest far-infrared turnovers, as shown in subsection 4.4, because their dust has a warmer temperature distribution, as seen is subsection 4.3. Thus we expect a systematic trend of infrared SEDs with total luminosity. Spinoglio et al. (1995) already showed that the higher the bolometric luminosity of a galaxy, the higher its ratio of starburst/cool dust components.

Indeed we do find that the far-infrared turnover becomes systematically sharper in the more luminous galaxies. This can be seen in the inverse correlation between the color index [200 - 100] and the 12μm luminosity, shown in Fig. 17. In this figure we see that this relation holds in general, irrespective of the type of the galaxy, with a regression coefficient of R=-0.48 for 81 objects, for all the observed galaxies in the 12μm sample, excluding the 3C and PG quasars. The fit to the non-Seyfert galaxies only is:

$$[200 - 100] = 13.513 - 0.317 \times Log(L_{12\mu m}) \tag{8}$$

(the linear regression coefficient is -0.52 for 26 data points).

We also plot in Fig.18 the inverse correlation between the color index [200 - 100] and the 60μm luminosity, which gives a regression coefficient of R=-0.48 for 83 objects, for all the galaxies in our sample, excluding the 3C and PG quasars. The fit for the non-Seyfert's only gives:

$$[200 - 100] = 14.983 - 0.346 \times Log(L_{60\mu m}) \tag{9}$$

(the linear regression coefficient is -0.63 for 26 data points)

The four most noticeable outliers are the two 3C objects and the two PG quasars, which have unexpectedly red [200 - 100] colors . There is therefore an indication that even at low redshift ($z \leq 0.2$) quasars (either the optically selected PG and the radio selected 3C) might have an excess in cold dust emission.

In Figures 19 and 20, we separate this color-luminosity trend into the slopes between 100 and 150μm and 150 to 200μm. Clearly the trend is due entirely to the steepening of the 200–150μm slope in the more luminous galaxies, which is the same whether the luminosity is measured at 12 or at 60μm. The 100–150μm slope in fact shows no significant luminosity dependence.

6. SUMMARY

New ISOPHOT photometry of a large sample of nearby active and normal galaxies shows that:

i) The 60-200μm SEDs of active and normal galaxies are similar. The 100 to 150 to 200μm spectra have significant curvature, generally downward. The trends are sufficiently systematic that measurements at these wavelengths can give accurate predictions of the fluxes at the intermediate wavelengths of 120, 170 and 180 μm.

ii) In the non-Seyfert galaxies, higher luminosities (presumably generated by higher rates of recent star formation) are correlated with hotter average dust temperatures at all wavelengths from 12 to 200μm. In particular, the 150 to 200μm slope steepens in more luminous galaxies.

iii) The decomposition of the observed SEDs into physically distinct spectral components has been extended from the IRAS data (RRC) to our ISO results: a strong distinction is apparent out to 200μm between the the quiescent disk component and the starburst component. We suggest that these components represent the extremes of minimal and maximal recent star formation, found in the least and most luminous galaxies, respectively.

iv) The [200 - 100] versus [100 - 60] color-color diagram is able to separate the three types of galaxies: starburst galaxies, normal galaxies and nearby spirals, while Seyfert's are at intermediate locations. The large-aperture 60–200 μm spectra of Seyfert galaxies we measured are dominated by the emission from the host galaxy. They therefore depend on the relative contributions of "starburst" and "quiescent disk" emission in the galaxy, and are independent of the presence of an active nucleus.

v) The [200 - 100] vs [60 - 25] color-color diagram shows that a mixture of two black-bodies with a warm and a cold component is able to fit all the far-infrared data, only if we assume the dust emissivity law proportional to the inverse square of the wavelength. Comparing active galaxies, Seyfert 1's show the larger range in temperature (22-70K), Seyfert 2's are intermediate, while starburst galaxies have the narrower range in dust temperature (30-60K). Nearby normal spirals and some of the CfA Seyfert galaxies show very cold dust components (15-18K).

vi) A correlation is found between the slope of the far-infrared turnover (as measured from the [200 - 100] color) and both the 60μm excess and the 12 and 60μm luminosities. We have confirmed and extended the finding of S95 that increasing star formation rates

cause the more luminous non-Seyfert galaxies to have relatively stronger 25–60μm emission, resulting in systematically bluer far-infrared colors. We suggest that the plane defined by the [200 - 100] color versus the 60μm excess can be used to separate *starburst dominated* galaxies from *AGN dominated* ones.

This research was funded in Italy from the Italian Space Agency (ASI). This work benefited from extensive use of the NASA Extragalactic Database (NED) and from the help given by the IPAC staff in planning the ISO observations. We thank Brian Rush and Nao Suzuki for help in preparing the observing command templates. We also thank the anonymous referee, whose thorough comments helped in improving this article.

A. DATA OBTAINED WITH THE ISOPHOT C100 ARRAY CAMERA

Some C100 observations, namely for objects FSC00521-7054, NGC 7674, MCG+1-33-36, NGC 262, FSC03362-1642, ESO253-G3, NGC 1365, NGC 4501, NGC 4922A/B were performed in staring mode, however only for the latter three an adjacent empty sky position was observed to measure the sky background. In the former cases sky background was estimated as follows: we assume that the sources are point-like and therefore only the central pixel (# 5) contains the source flux. The adjacent pixels were averaged to get a background value, which was then subtracted from the signal of the central pixel. This procedure is, however, affected by large uncertainties since it requires a good flat-fielding of the array because of its unstable behavior and in two cases, for NGC 7674 and NGC 262, the values inferred are much lower than the corresponding IRAS photometry. Note that the uncertainties quoted here are only the statistical ones. The results of the C100 observations are reported in Table 5.

REFERENCES

Alexander D.M. and Aussel, H., 1999, in ISO Surveys of a Dusty Universe, Eds. D. Lemke, M. Stickel & K. Wilke , Springer Lecture Notes of Physics Series, 548, 117.

Alton, P.B., et al.1998, A&A, 335, 807

Antonucci, R. 1993, ARA&A, 31, 473

Calzetti, D., Armus, L., Bohlin, R.C.,Kinney, A.L., Koornneef, J. Storchi-Bergmann, T. 2000, ApJ, 533, 682

Edelson, R.A. & Malkan, M.A. 1986, ApJ, 308, 59.

Edelson, R.A., Malkan, M.A. & Rieke, G.H. 1987, ApJ, 321, 233

Fang, F., Shupe, D.L., Xu, C., Hacking, P.B. 1998, ApJ, 500, 693

Franceschini A., Aussel H., Cesarsky C.J., Elbaz, D., Fadda, D. 2001, A&A, 378, 1

Gabriel, C., Acosta-Pulido, J., Heinrichsen, I., Morris, H., Tai, W.-M. 1997, in ASP Conf. Ser. 125, Astronomical Data Analysis Software and Systems VI, ed. Gareth Hunt and H. E. Payne, eds., 108

Genzel, R. et al. 1998, ApJ, 498, 579

Genzel, R. & Cesarsky, C.J. 2000, ARA&A, 38, 761

Granato, G.L., & Danese, L., 1994, MNRAS, 268, 235

Haas, M., Muller, S.A.H., Chini, R., Meisenheimer, K., Klaas, U., Lemke, D., Kreysa, E., Camenzind, M. 2000, A&A, 354, 453

Huchra, J. & Burg, R. 1992, ApJ, 393, 90

Kessler M.F., et al. 1996, A&A, 315, L27

Klaas, U., Haas, M., Heinrichsen, I., Schulz, B. 1997, A&A325, L21

IRAS Point Source Catalog, Version 2, 1988, Joint IRAS Science Working Group (Washington, DC: GPO).

Lemke D. et al. 1996, A&A315, L64

Laureijs R.J. et al. 2001, The ISO Handbook, Vol.V, The Imaging Photo-polarimeter, SAI/99-069/Dc, Version 1.2, July 1, 2001, T. Muller & J. Blommaert Eds.(available also at http://www.iso.vilspa.esa.es/manuals/HANDBOOK/V/pht_hb/)

Maiolino, R., Ruitz, M., Rieke, G.H., Keller, L.D. 1995, ApJ, 446, 561

Malkan, M. 2001, preprint astro-ph/0110357, from Kyoto Cosmology Conference in honor of Prof. Tomita.

Malkan, M. 2000, in "Birth and Evolution of the Universe", Proceedings of Fourth RESCEU International Symposium, eds. K. Sato and M. Kawasaki (Universal Academy Press; Tokyo), p. 119 (also available as astro-ph/0005251).

Meisenheimer, K., Haas, M., Müller, S.A.H., Chini, R., Klaas, U., Lemke, D. 2001, A&A, 372, 719

Moshir, M. et al. 1992, Explanatory Supplement to the IRAS Faint Source Survey, version 2, JPL D-10015 8/92 (Pasadena: JPL).

Pérez García, A.M. & Rodríguez Espinosa, J.M. 2000, ApJ, 557, 39 (PGRE)

Polletta, M. & Courvoisier, T.J.-L., 1999, A&A, 350, 765

Polletta, M., Courvoisier, T.J.-L.,Hooper, E.J., Wilkes, B.J. 2000, A&A, 362, 75

Radovich, M., Klaas, U., Acosta-Pulido, J., Lemke, D. 1999, A&A, 348, 705

Rowan-Robinson, M., and Crawford, J. 1989, MNRAS, 238, 523 (RRC)

Rush, B., Malkan, M.A. & Spinoglio, L. 1993, ApJS, 89,1 (RMS)

Siebenmorgen, R., Krugel, E., Chini, R. 1999, A&A, 351, 495

Schmidt, M. & Green, R.F. 1983, ApJ, 269, 352

Spinoglio, L., Malkan, M.A., Rush B., Carrasco, L., Recillas-Cruz, E. 1995, ApJ, 453, 616 (S95)

Spinoglio, L. & Malkan, M.A. 1989, ApJ, 342, 83

Thean, A., Pedlar, A., Kukula, M.J., Baum, S.A., O'Dea, C.P. 2000, MNRAS, 314, 573

Thean, A., Pedlar, A., Kukula, M.J., Baum, S.A., O'Dea, C.P. 2001 MNRAS, 325, 737

Xu, C., et al. 1998, ApJ, 508, 576

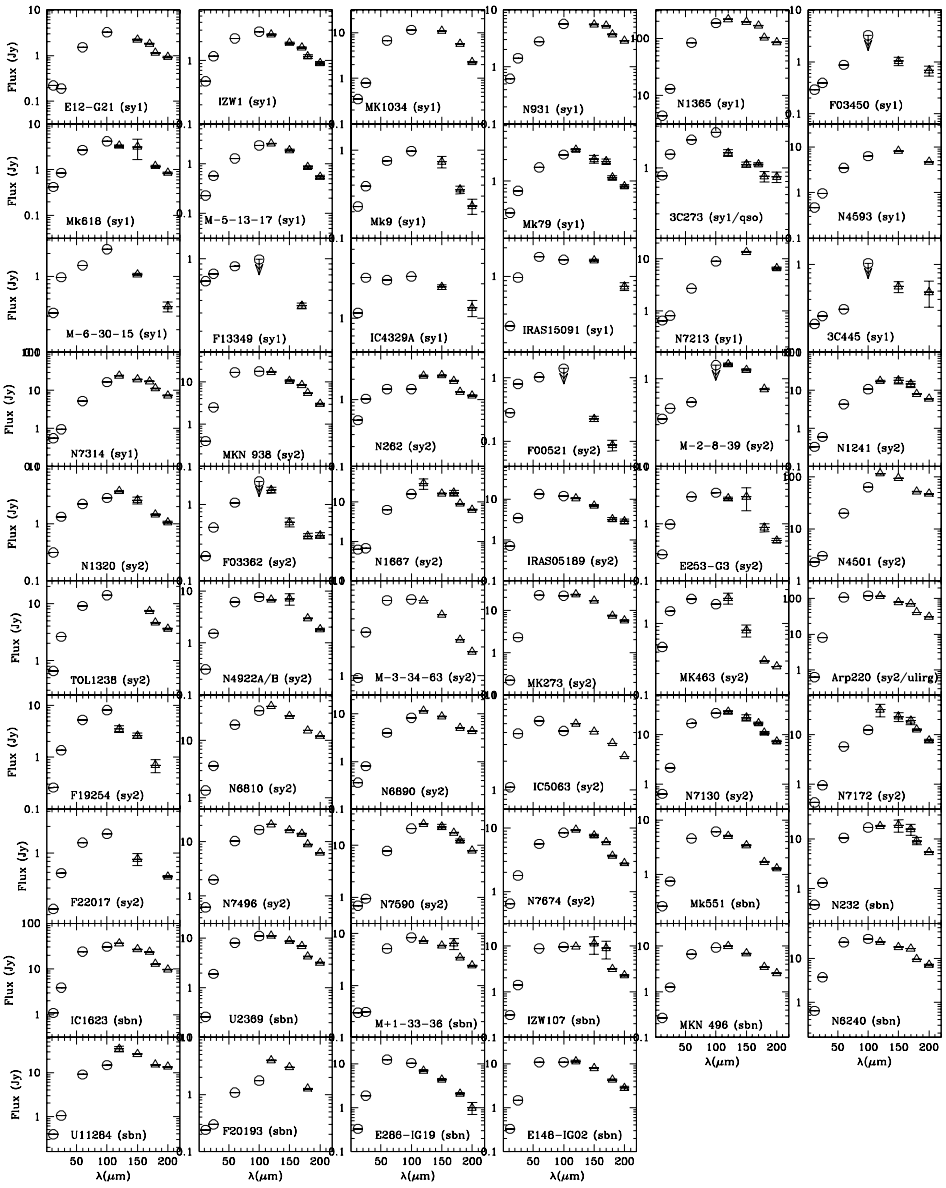

Fig. 1.— ISOPHOT data (open triangles) and IRAS fluxes (open circles) from RMS.

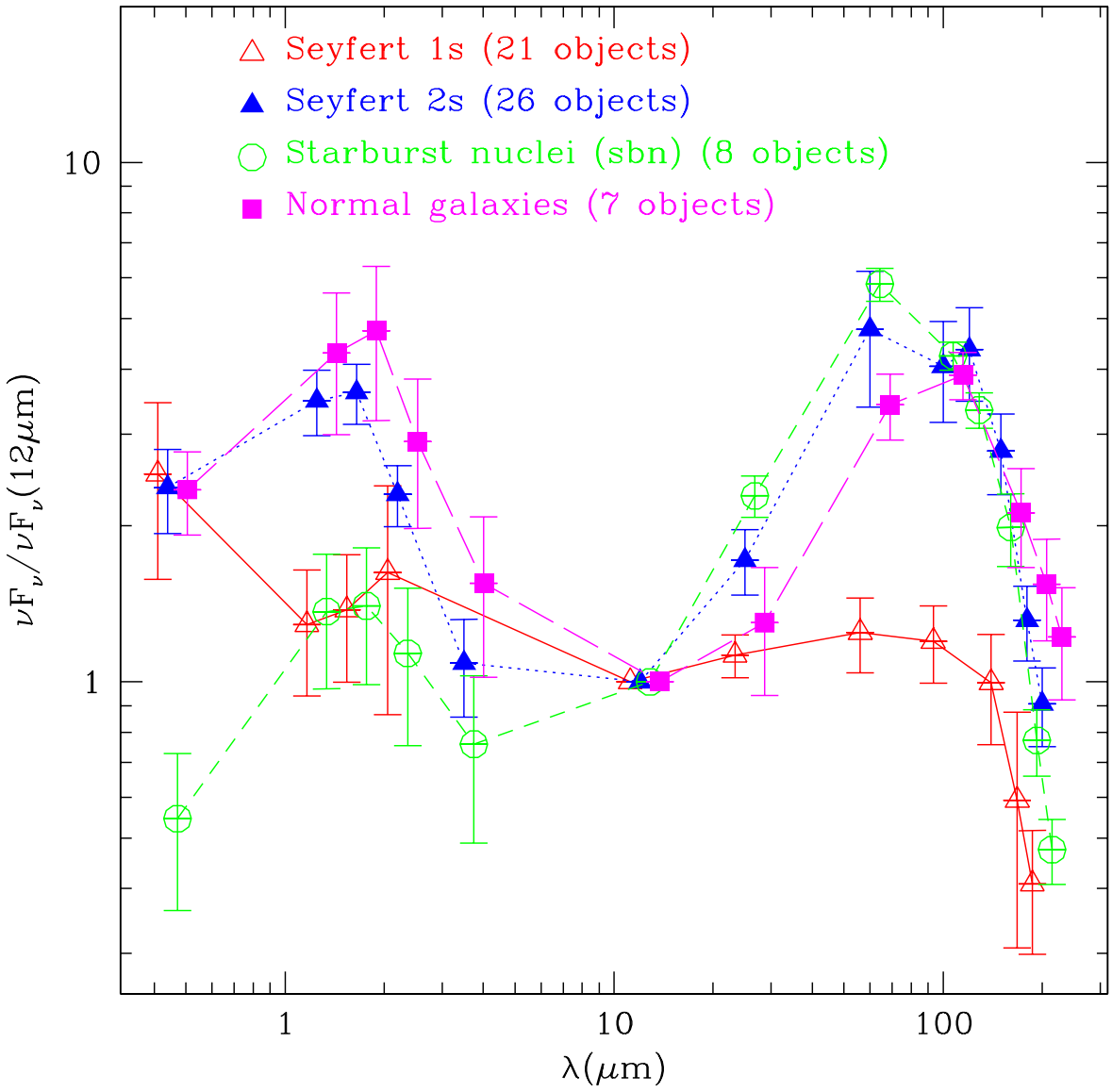

Fig. 2.— Combined SEDs of active and normal galaxies of the 12μm sample from 4400Å to 200μm, normalized to 12μm (Note that the number of objects plotted here is smaller than the total number of galaxies because some of then do not have near-infrared and/or optical data in S95. Note also that the 170μm band has been excluded from the average values in this figure and in the following Fig.3,4 and 6 because the statistics is poor, as can be seen from Table 2).

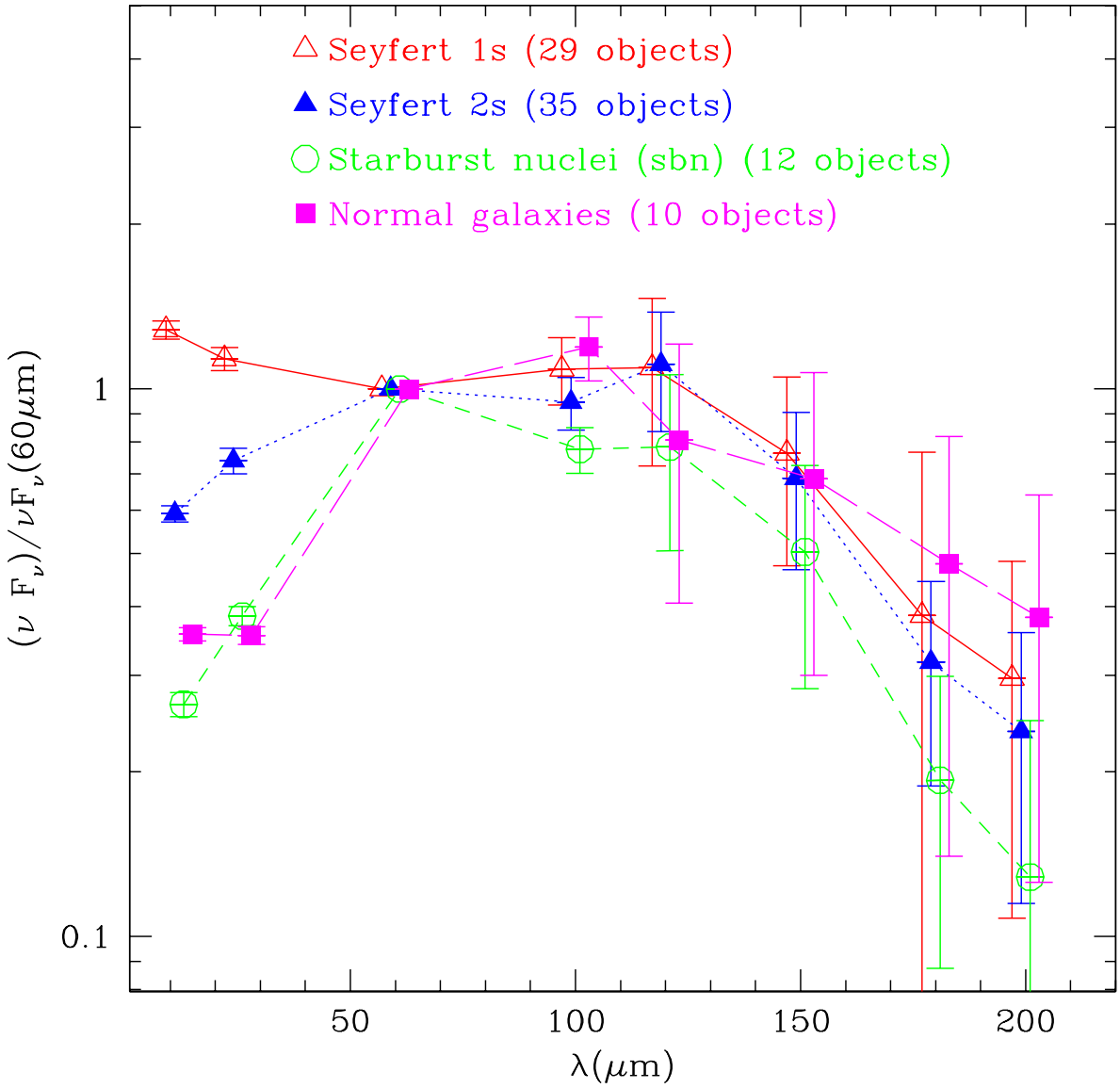

Fig. 3.— The average SED normalized to $60\mu m$ of galaxies belonging to the $12\mu m$ galaxy sample. The nearby spirals class has been excluded, because of poor statistics.

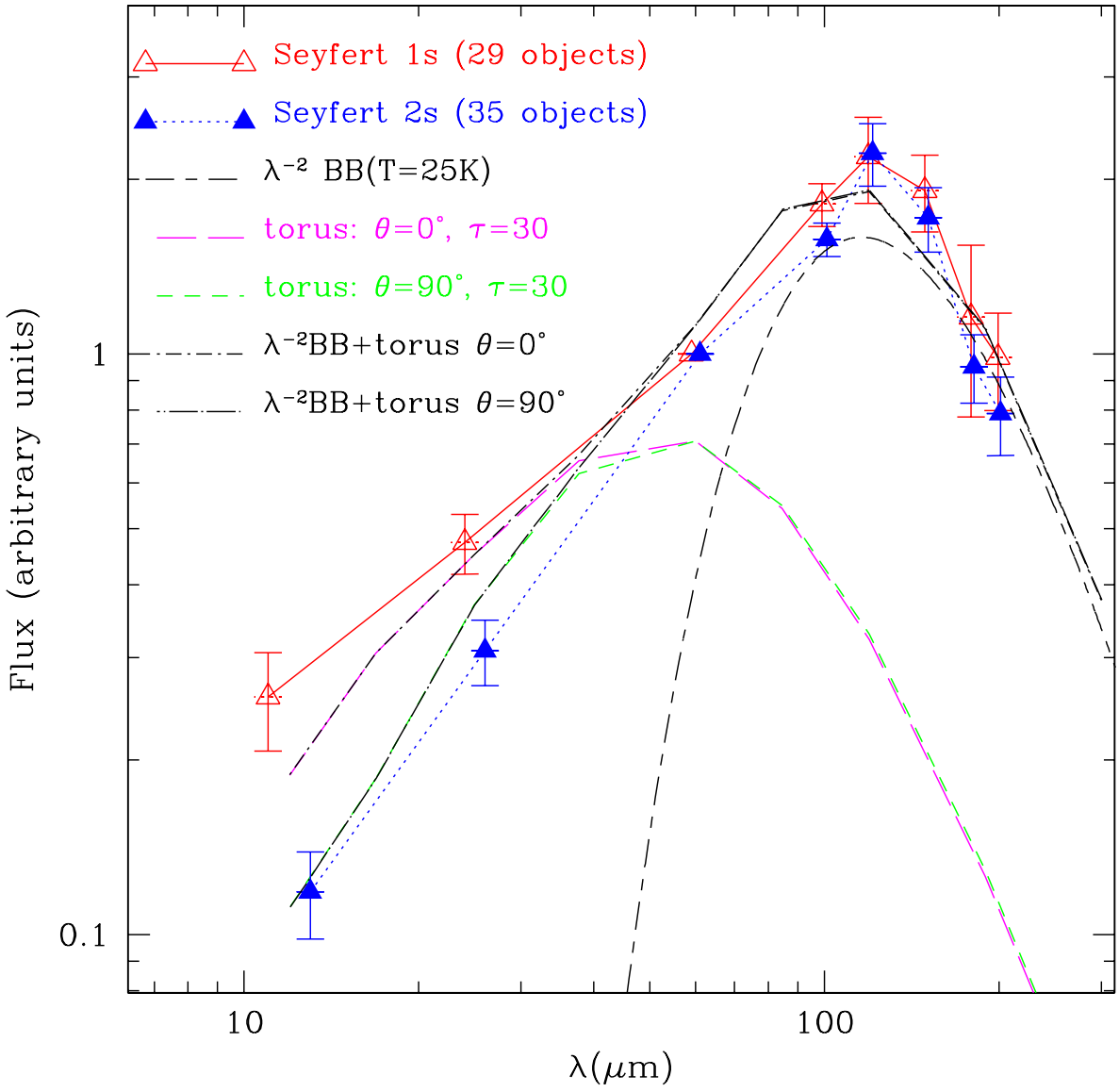

Fig. 4.— Comparison between the average Seyfert 1's (open triangles) and 2's (filled triangles) SEDs. The short dashed line shows the edge-on model ($\theta = 90°$, $\tau = 30$); the long dashed line, the face-on model $\theta = 0°$, $\tau = 30$) from Granato & Danese (1994). The short and long dashed line shows the component of host-galaxy disk emission which was added to the torus models to match the overall SEDs of the Seyfert galaxies–it is approximated as grey-body emission at T=25K.

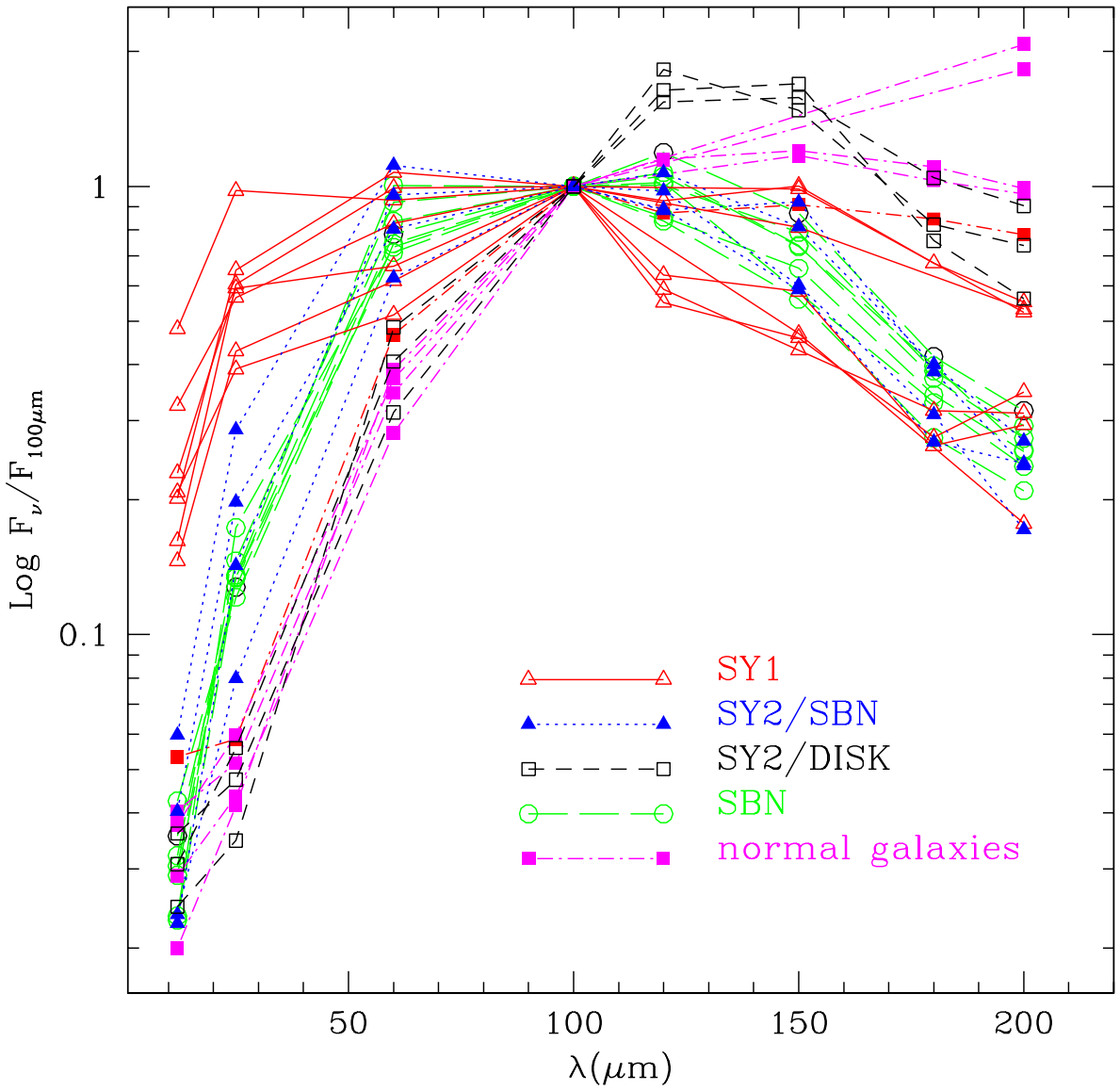

Fig. 5.— The flux densities normalized to the 100 μm flux density of the galaxies chosen to represent the different emission components. The chosen normal spiral galaxies are: NGC 7624, NGC 7083, UGC 2936, NGC 134 and NGC 5194 (M 51); the starburts galaxies are: IC 1623, MK 496, IZw 107, MK 551, UGC 2369, ESO 148-IG02 and NGC 6240; the Seyfert 1's are: FSC15091-2107, 3C 273, IC 4329A, MCG-6-30-15, NGC 4151, NGC 5548 and MK 817. Finally the Seyfert 2's with starburst SED are: FSC 05189-2524, MK 938, NGC 7130 and NGC 4922; while those with disk SED are: NGC 1241, NGC 4501 and NGC 3079. Note that the data at 170μm have been omitted because available only for few objects.

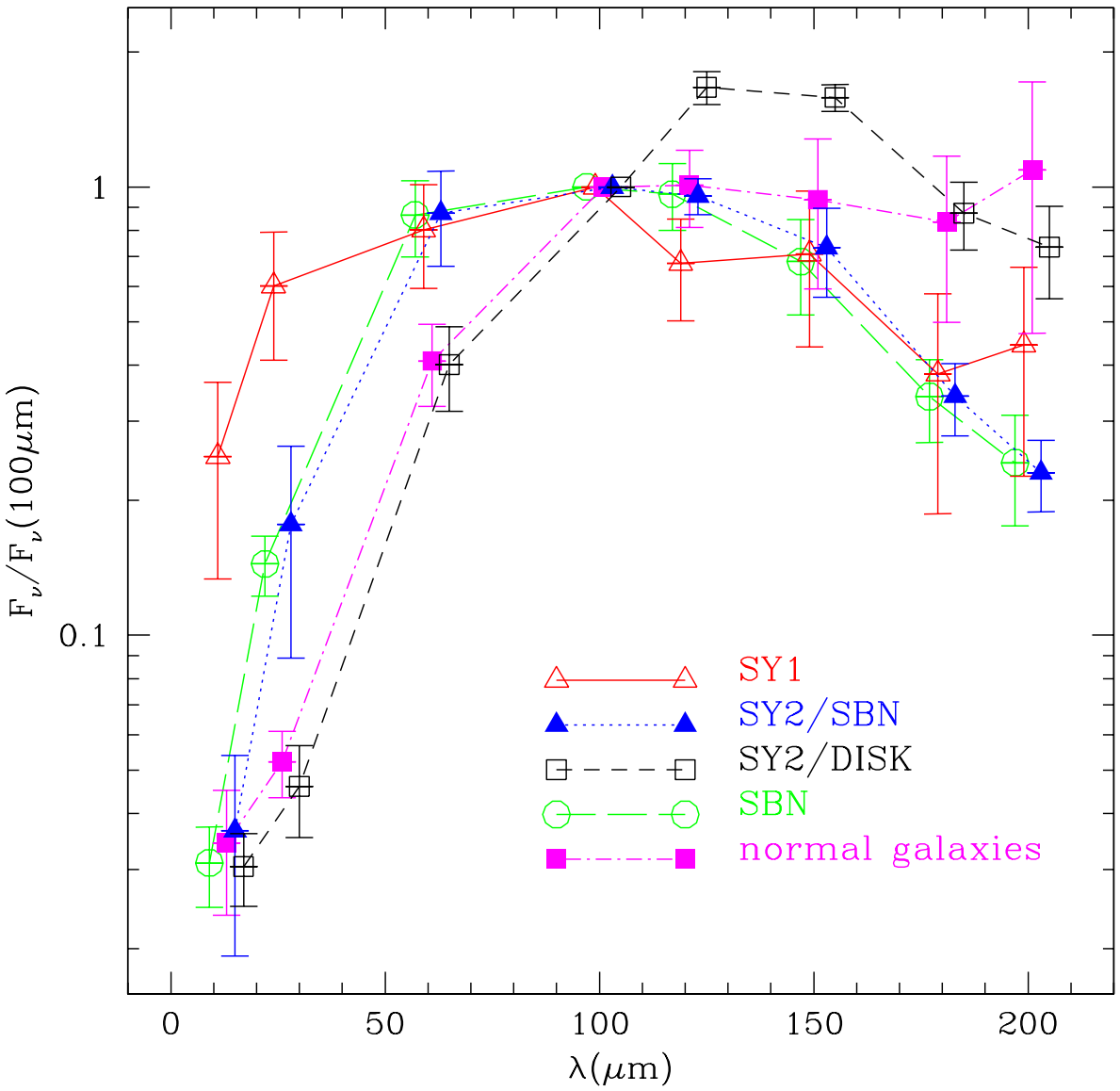

Fig. 6.— The average flux densities for each type of galaxies representing different emission components ("pure" Seyfert, starburst, disk emission, starburst-like Seyfert 2 and disk-like Seyfert 2). These are the averages of the data plotted in Figure 5, again normalized to the 100μm flux density.

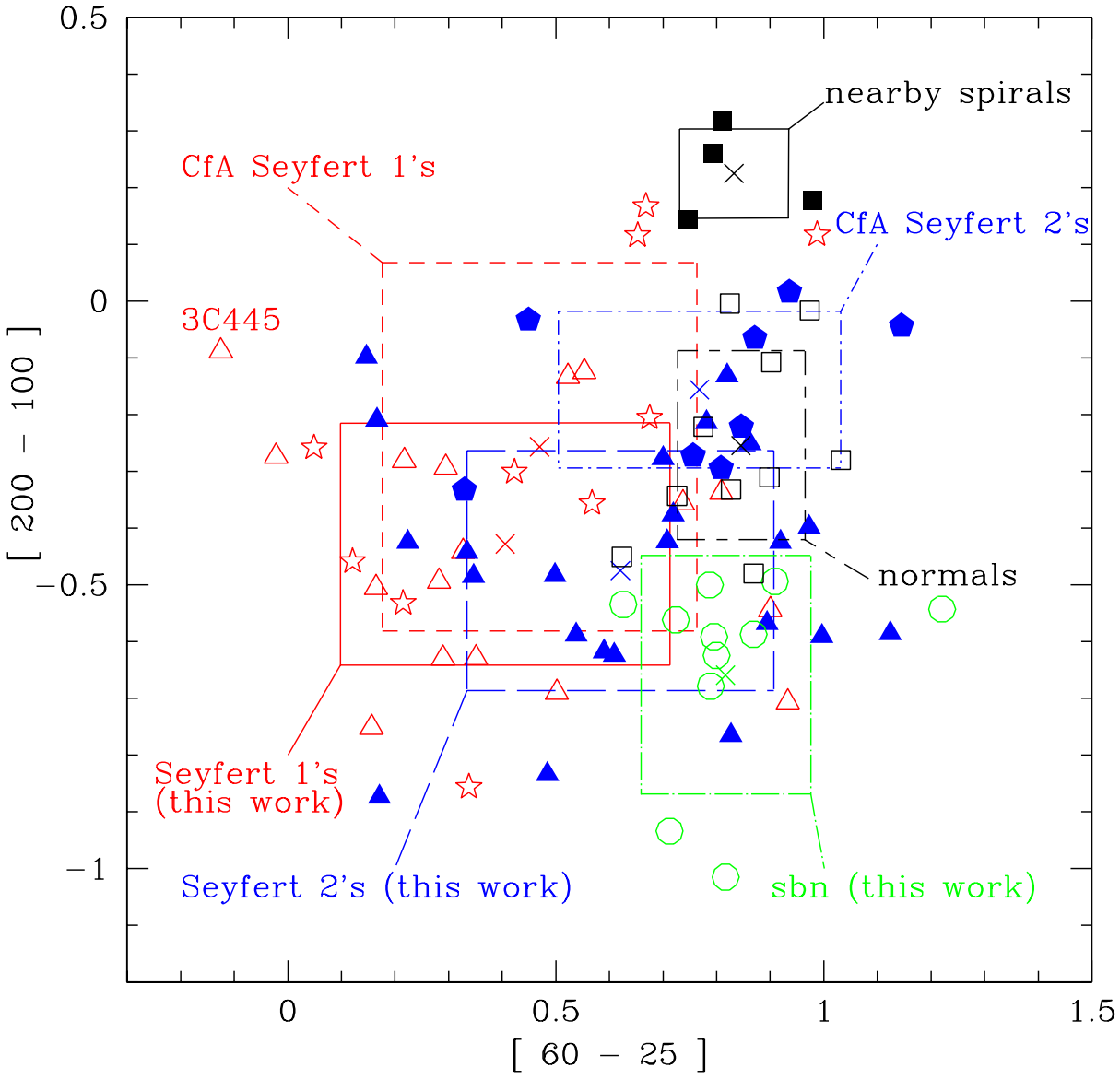

Fig. 7.— The [200 - 100] versus [60 - 25] color-color diagram of the various galaxies belonging to the 12μm galaxy sample. Open triangles represent Seyfert 1's, open stars are CfA Seyfert 1's (PGRE), filled triangles are Seyfert 2's, filled pentagons are CfA Seyfert 2's (PGRE), open circles are starburst nuclei, open squares are normal galaxies and filled squares are nearby spiral galaxies. The mean colors of each class of galaxies are indicated by crosses, with their 1σ dispersion shown by boxes.

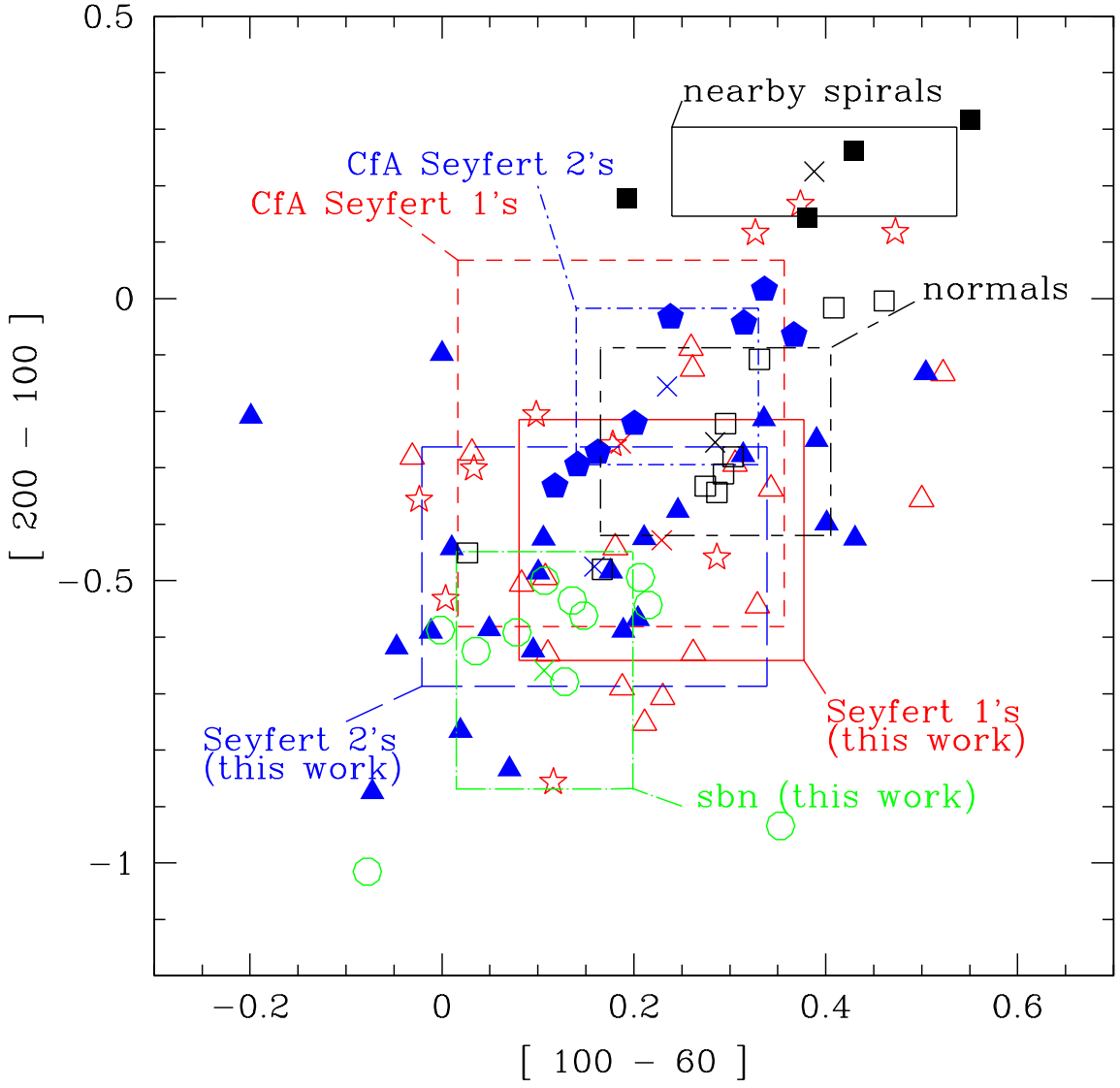

Fig. 8.— The [200 - 100] versus [100 - 60] color-color diagram of the various galaxies belonging to the 12μm galaxy sample. We refer to Fig.7 for the notation.

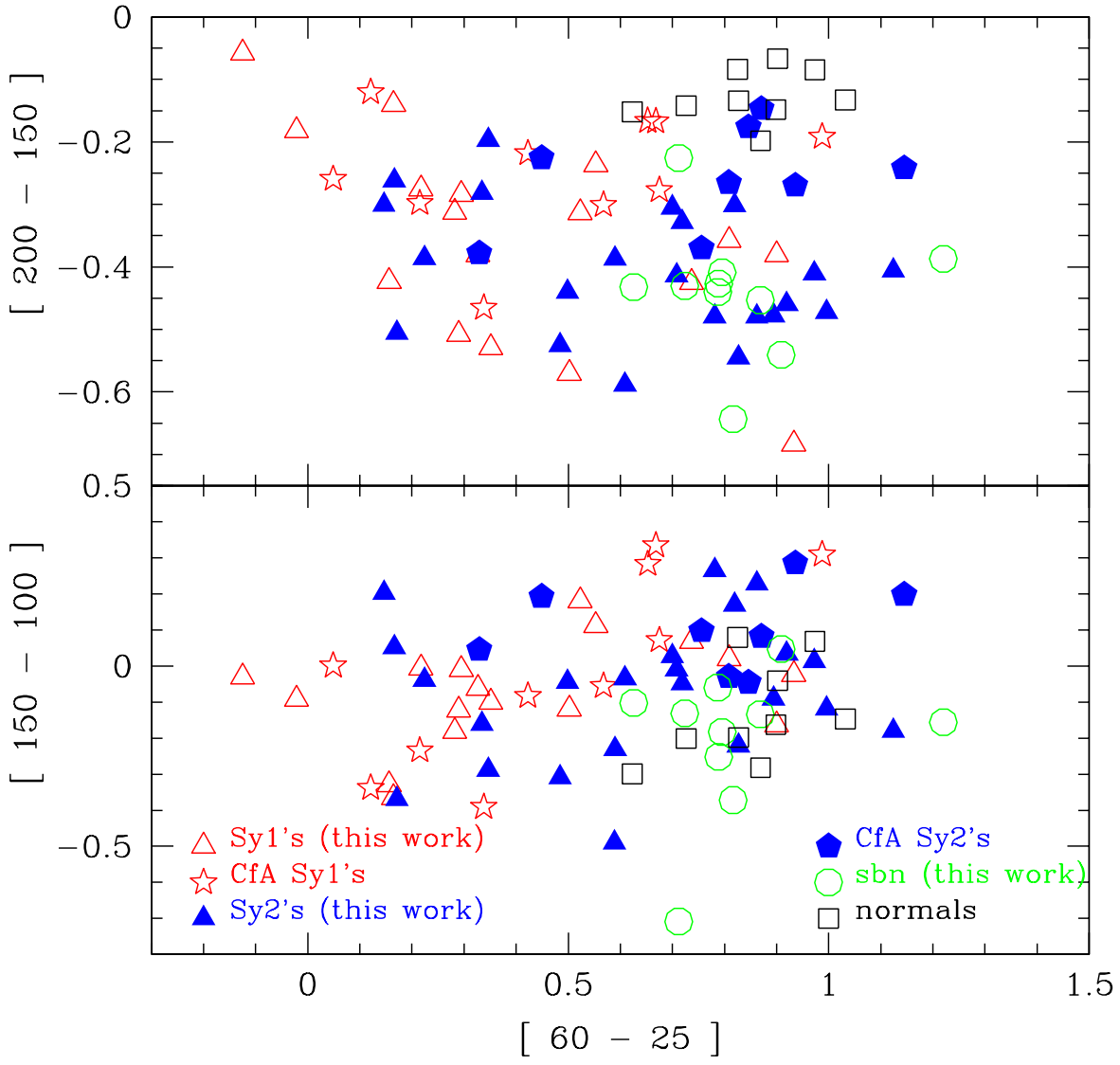

Fig. 9.— The far-infrared colors [150 - 100] (lower panel) and [200 - 150] (upper panel) versus the IRAS color [60 - 25].

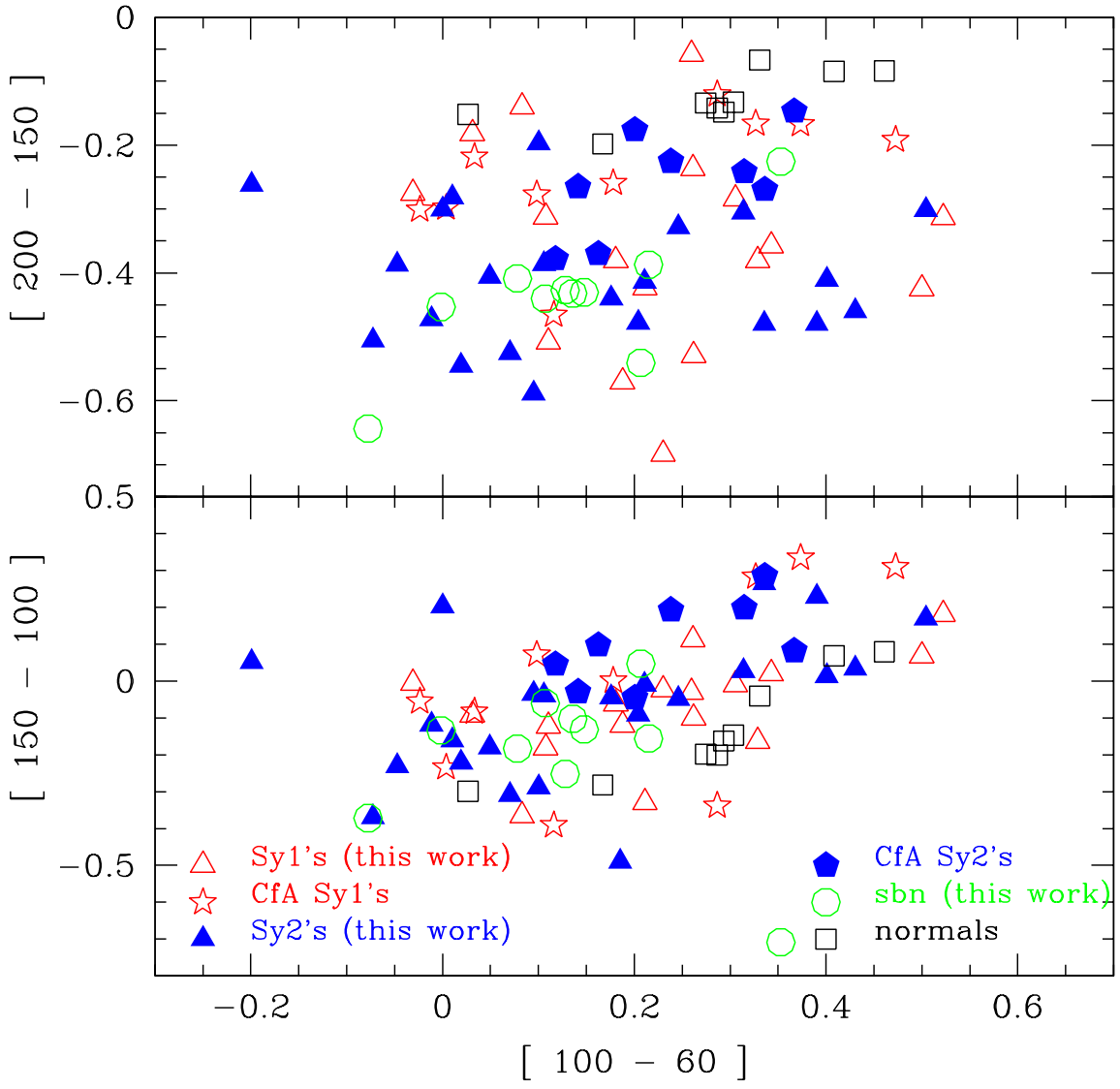

Fig. 10.— The far-infrared colors [150 - 100](lower panel) and [200 - 150] (upper panel) versus the IRAS color [100 - 60]

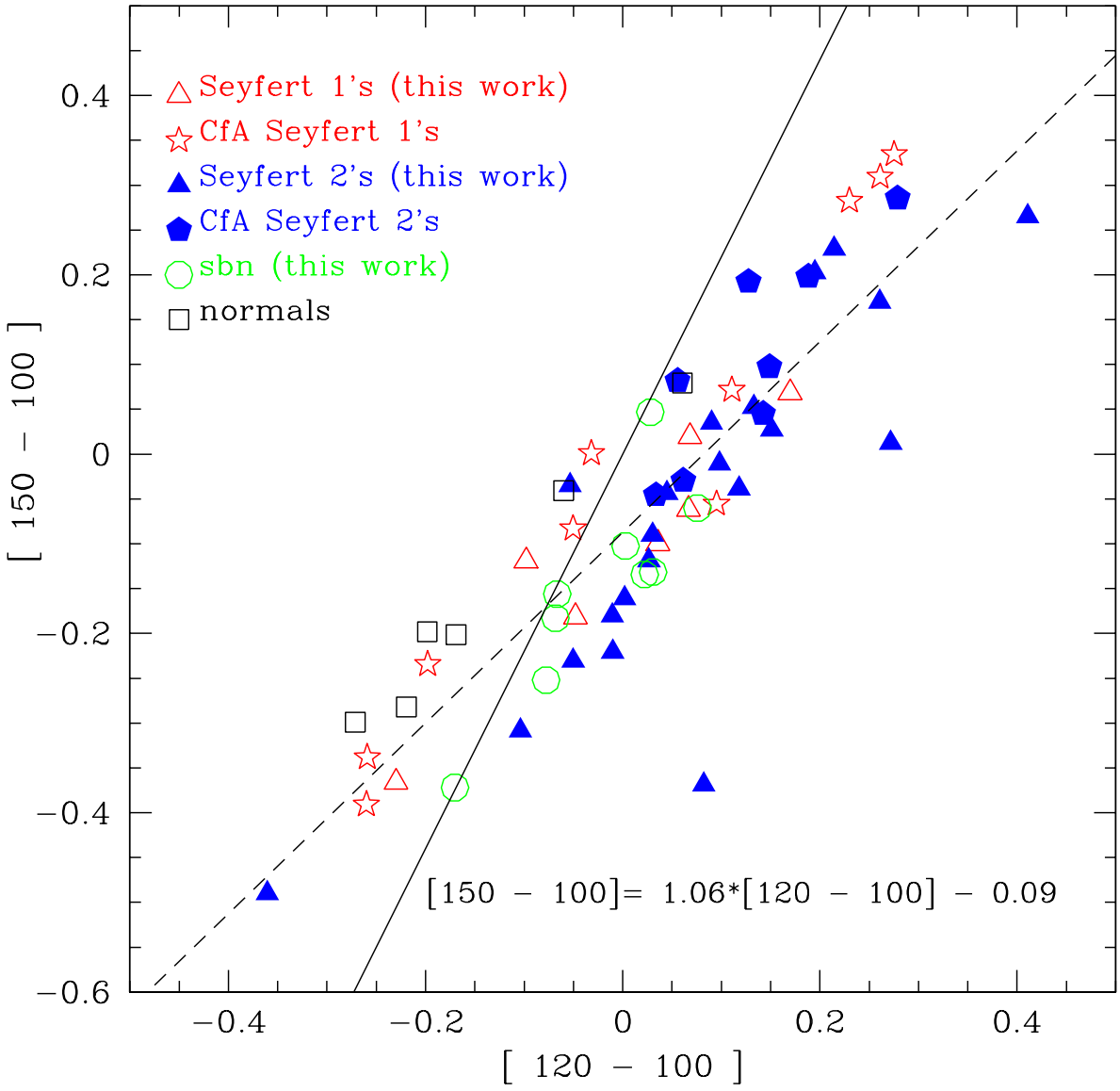

Fig. 11.— The [150 - 100] versus the [120 - 100] color-color diagram. The dashed line represents the least squares fit to the data, the solid line gives the locus of a pure power law spectral dependence of flux densities.

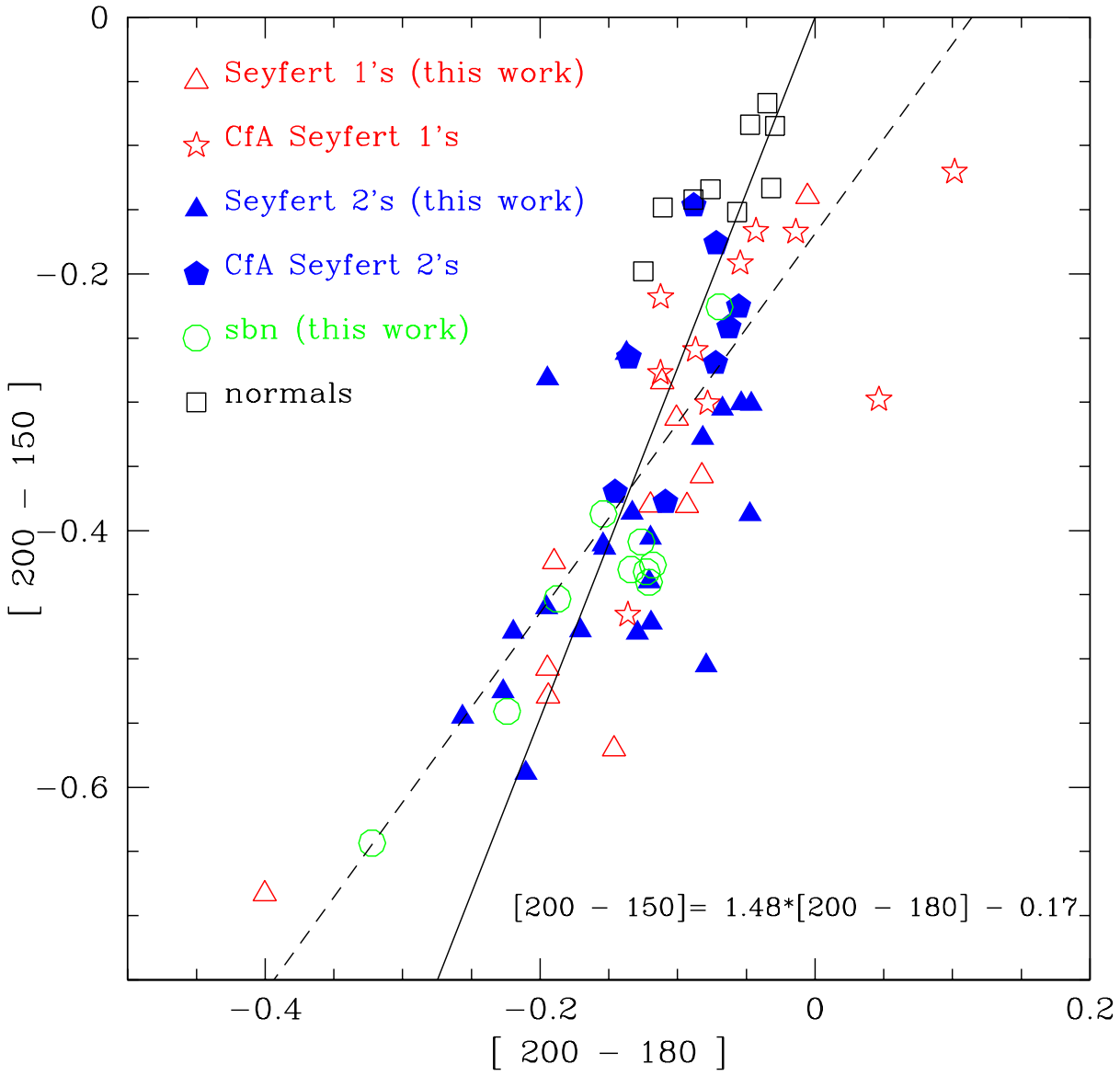

Fig. 12.— The [200 - 150] versus the [200 -180] color-color diagram. Dashed and solid line as for the previous figure.

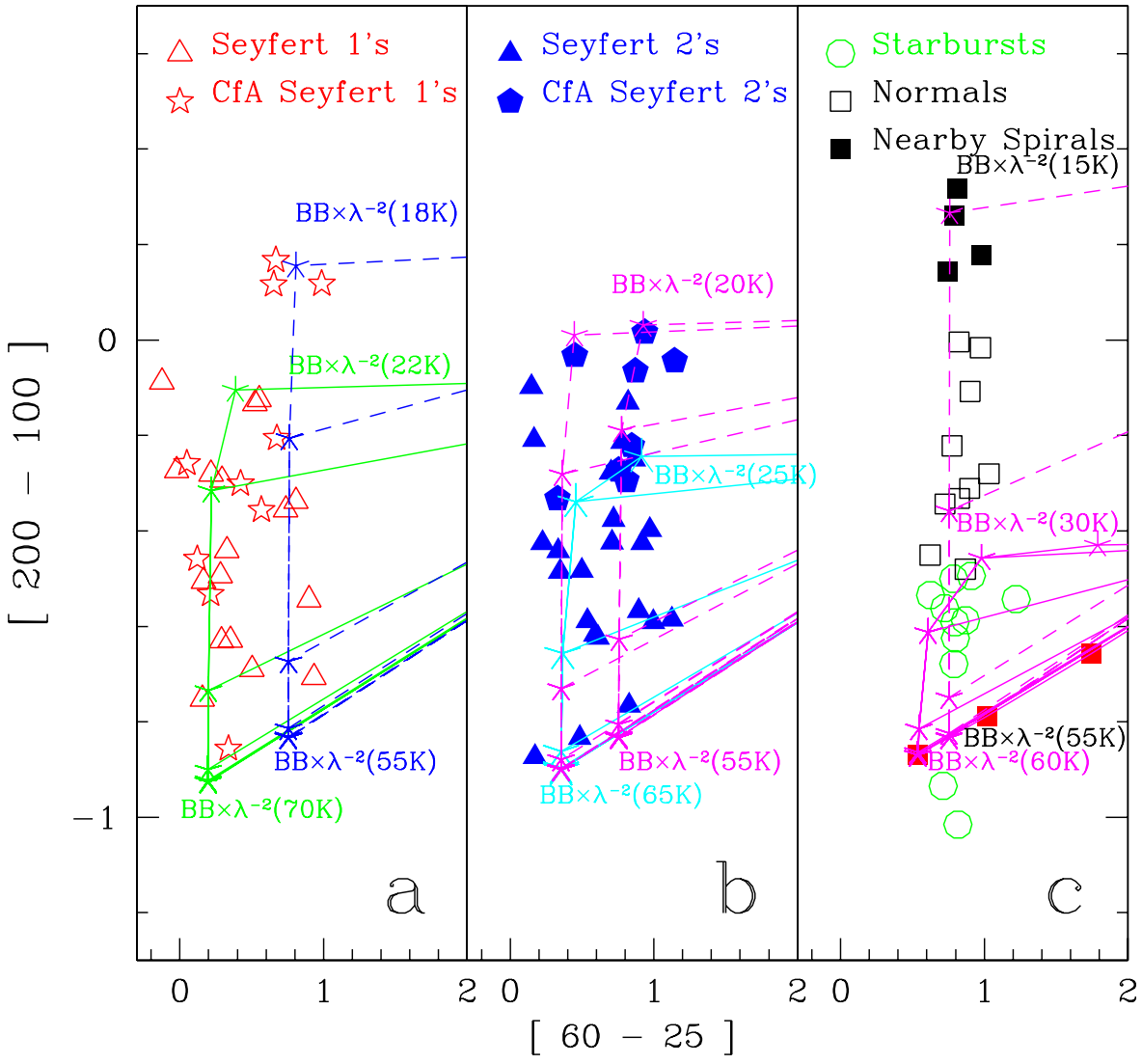

Fig. 13.— The [200 - 100] versus [60 - 25] color-color diagram of the various classes of galaxies belonging to the 12μm galaxy sample. a: Seyfert 1's galaxies. b: Seyfert 2's galaxies. c: starburst and normal galaxies. The lines represent the models made of the mixture of two black-bodies at the quoted temperatures (with λ^{-2} dust emissivity). The tracks running off to the right hand side are pointing to the locus of the "pure" low temperature grey-body.

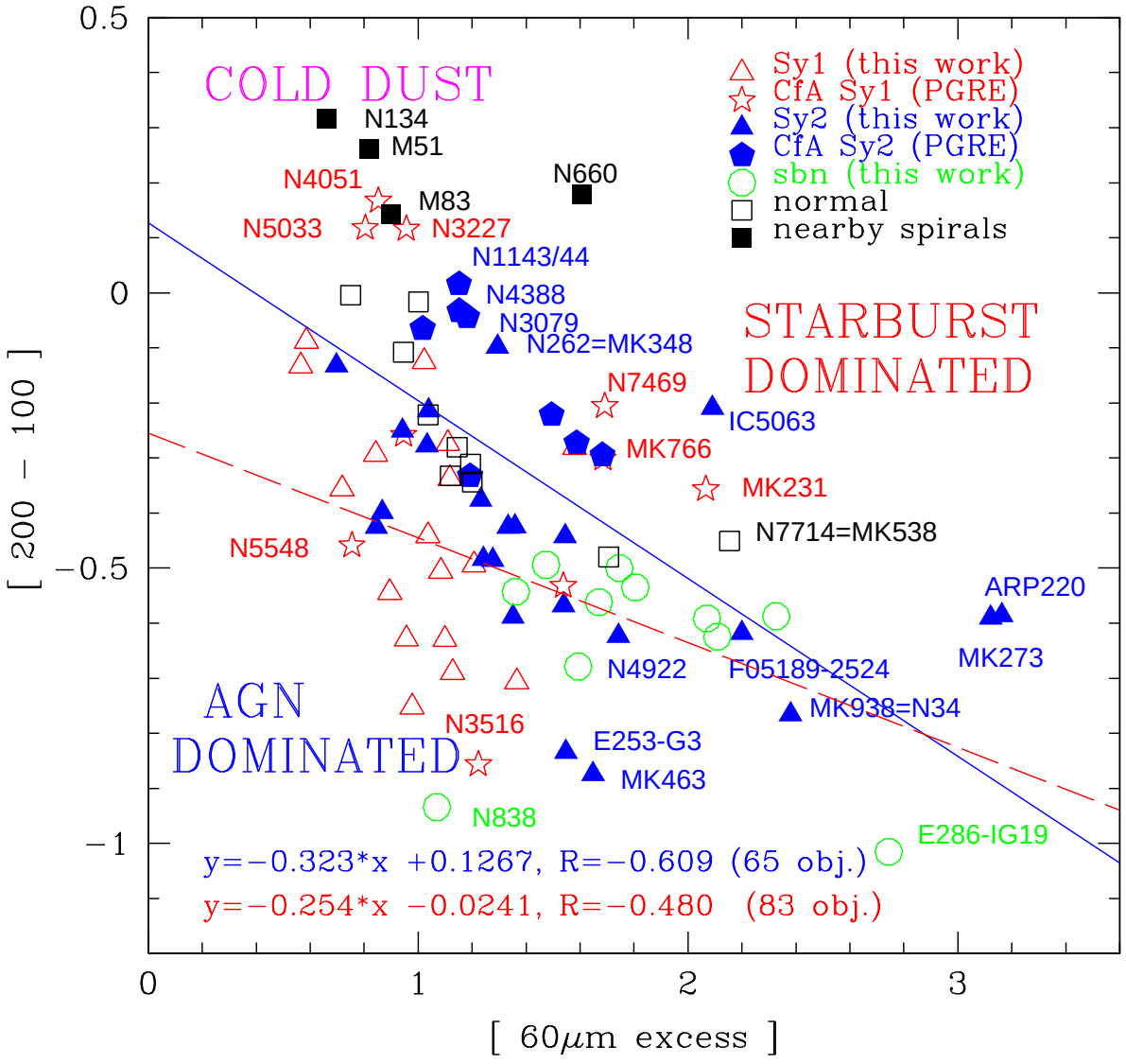

Fig. 14.— The [200 - 100] color versus the 60μm excess diagram of galaxies belonging to the 12μm galaxy sample. The data for 17 CfA Seyfert galaxies (PGRE), 10 normal galaxies (Siebenmorgen, Krugel & Chini 1999), 4 nearby spiral galaxies (Alton et al. 1998) and the Seyfert 2's NGC 7582 (Radovich et al. 1999), all belonging to the 12μm galaxy sample, are included. The broken line shows the linear fit to all the data of 12μm galaxies, while the solid line shows the fit of all but the Seyfert 1's (the regression coefficient is R=-0.480 for 83 data points and R=-0.609 for 65 points, respectively). The anti-correlation improves and becomes more steep excluding Seyfert 1's.

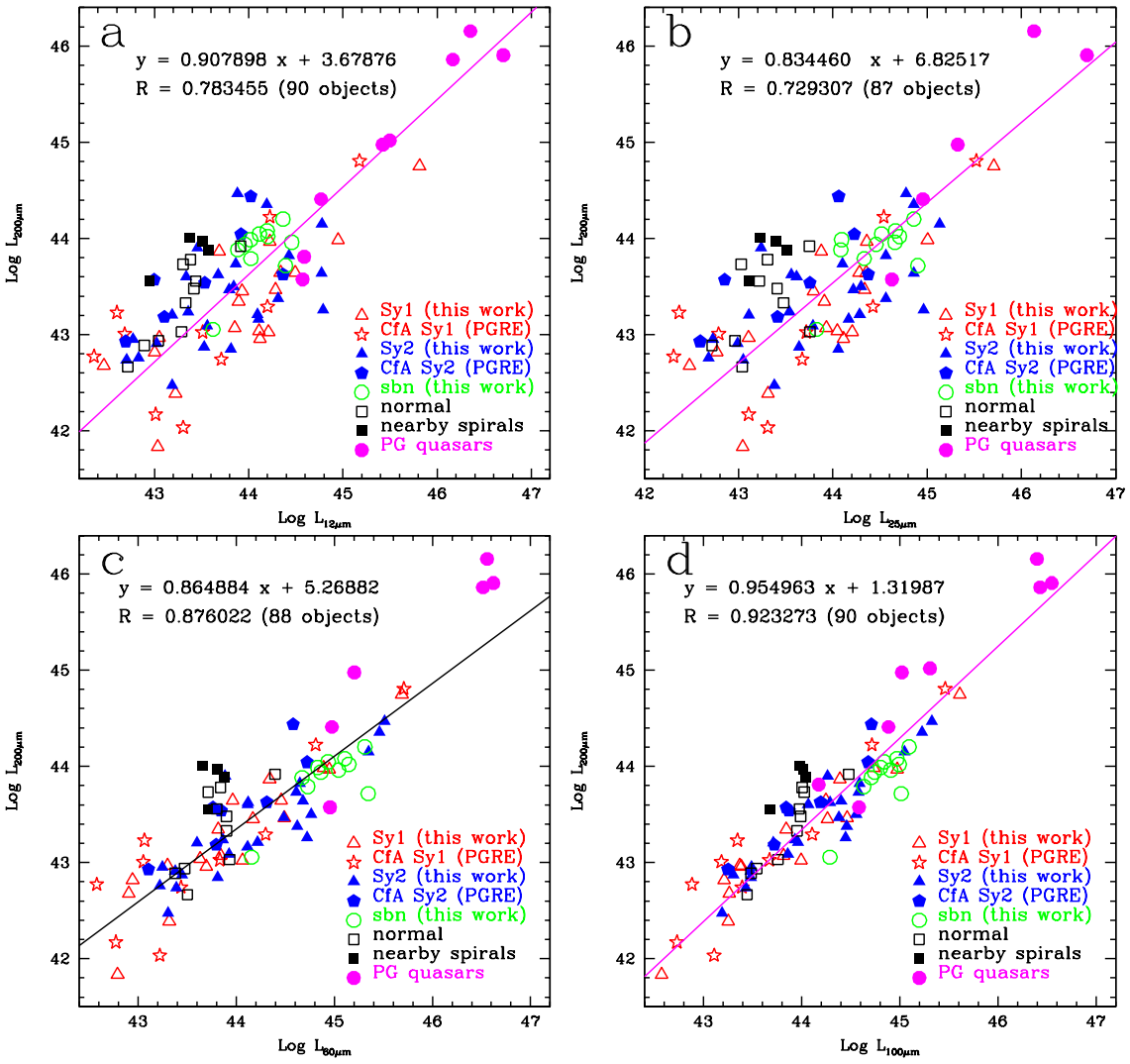

Fig. 15.— The 200 μm luminosity versus: (a) the 12 μm luminosity; (b) the 25 μm luminosity; (c) the 60 μm luminosity; (d) the 100 μm luminosity. Note that the luminosities (in this and in the following figures) are always in units of erg s^{-1}.

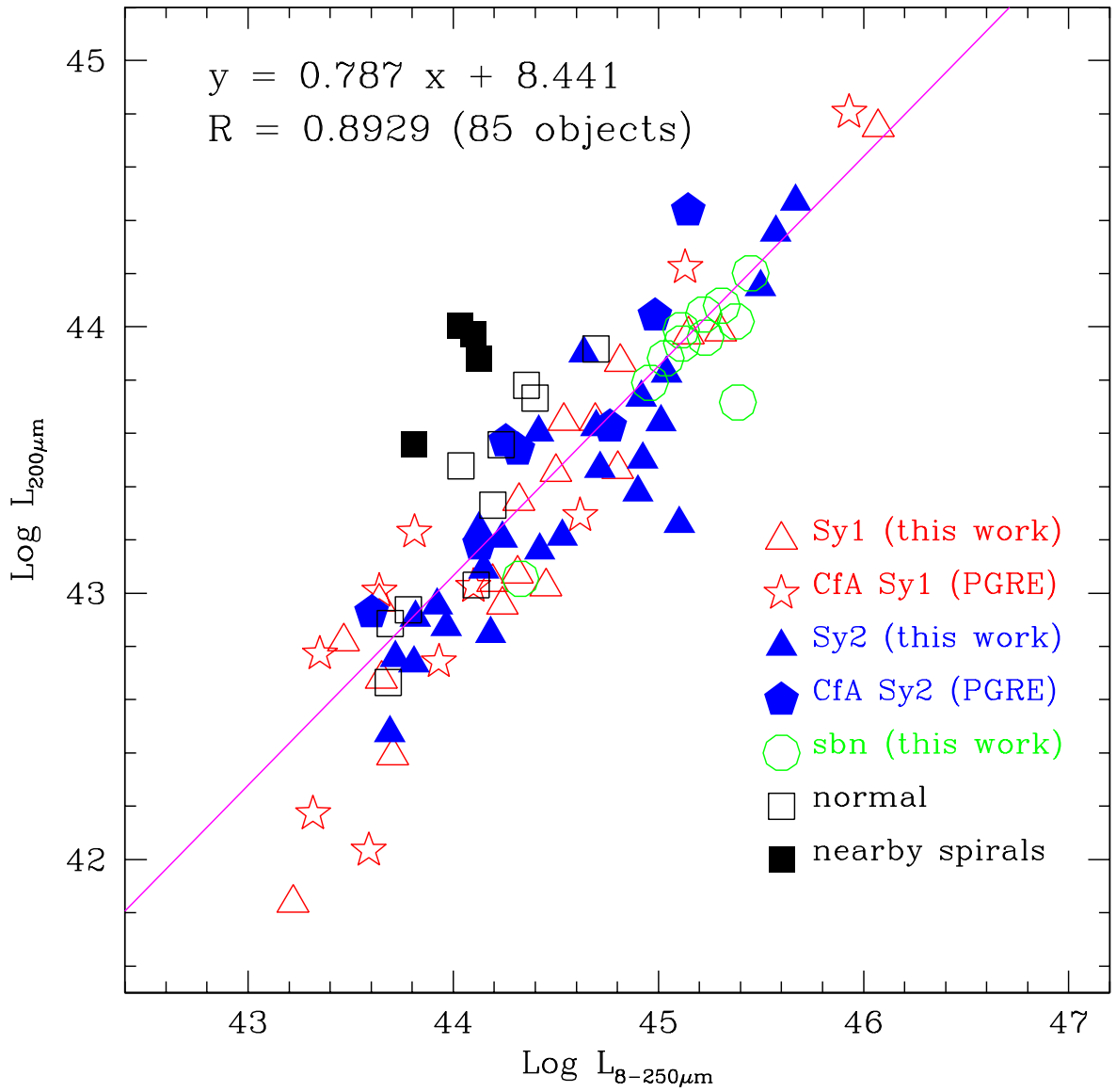

Fig. 16.— The 200 μm luminosity versus the total mid to far-infrared μm luminosity (given in Table 3).

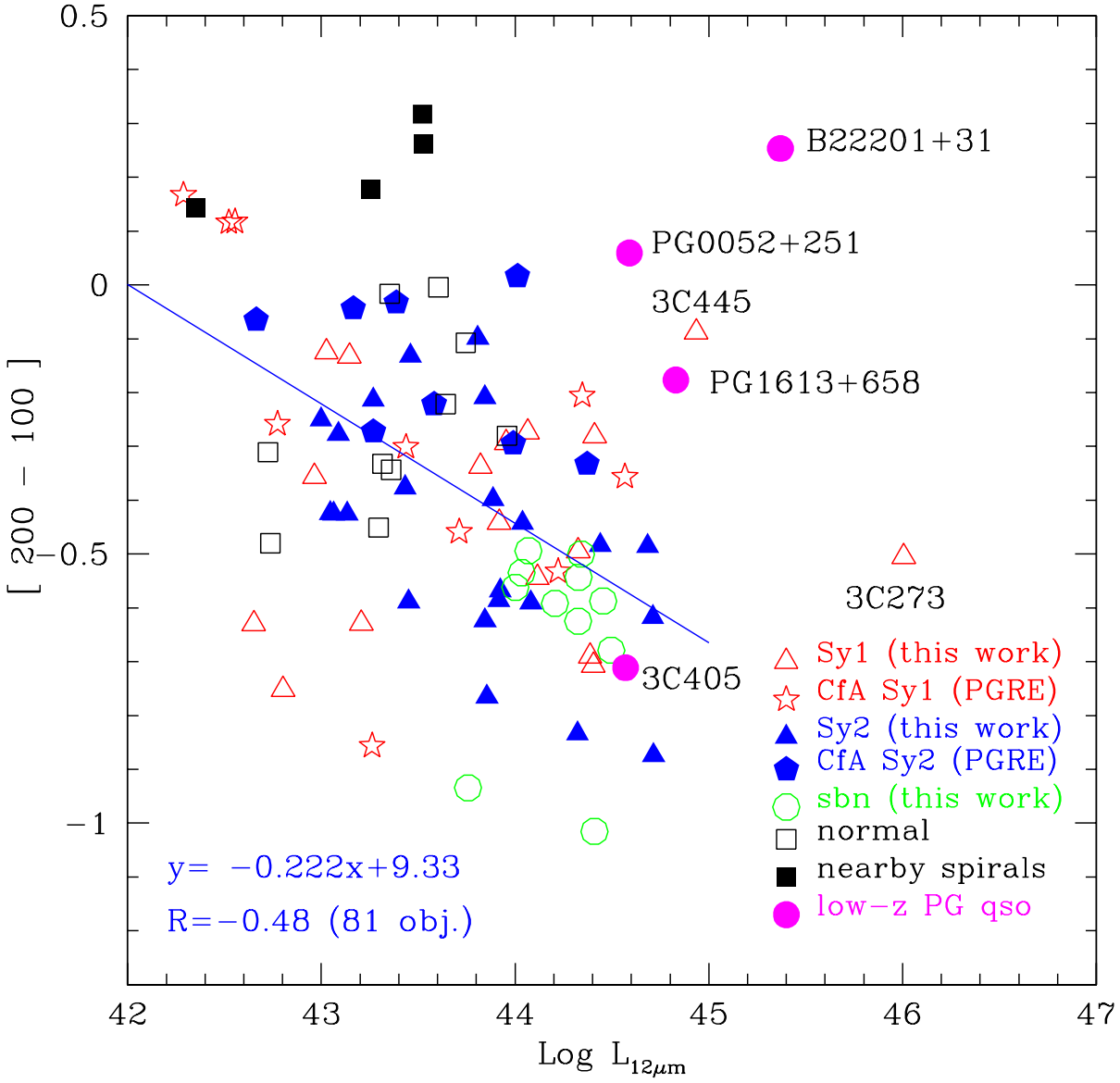

Fig. 17.— The [200 - 100] color versus the 12μm luminosity diagram of galaxies belonging to the 12μm galaxy sample. For comparison are also shown three low redshift (z $\leq$ 0.2) PG quasars and 3C405 (Haas et al. 2000). The solid line represents the linear fit that excludes the 3C objects and the PG quasars, showing a mild correlation between color and 12μm luminosity (the regression coefficient is R=-0.482 for 81 data points).

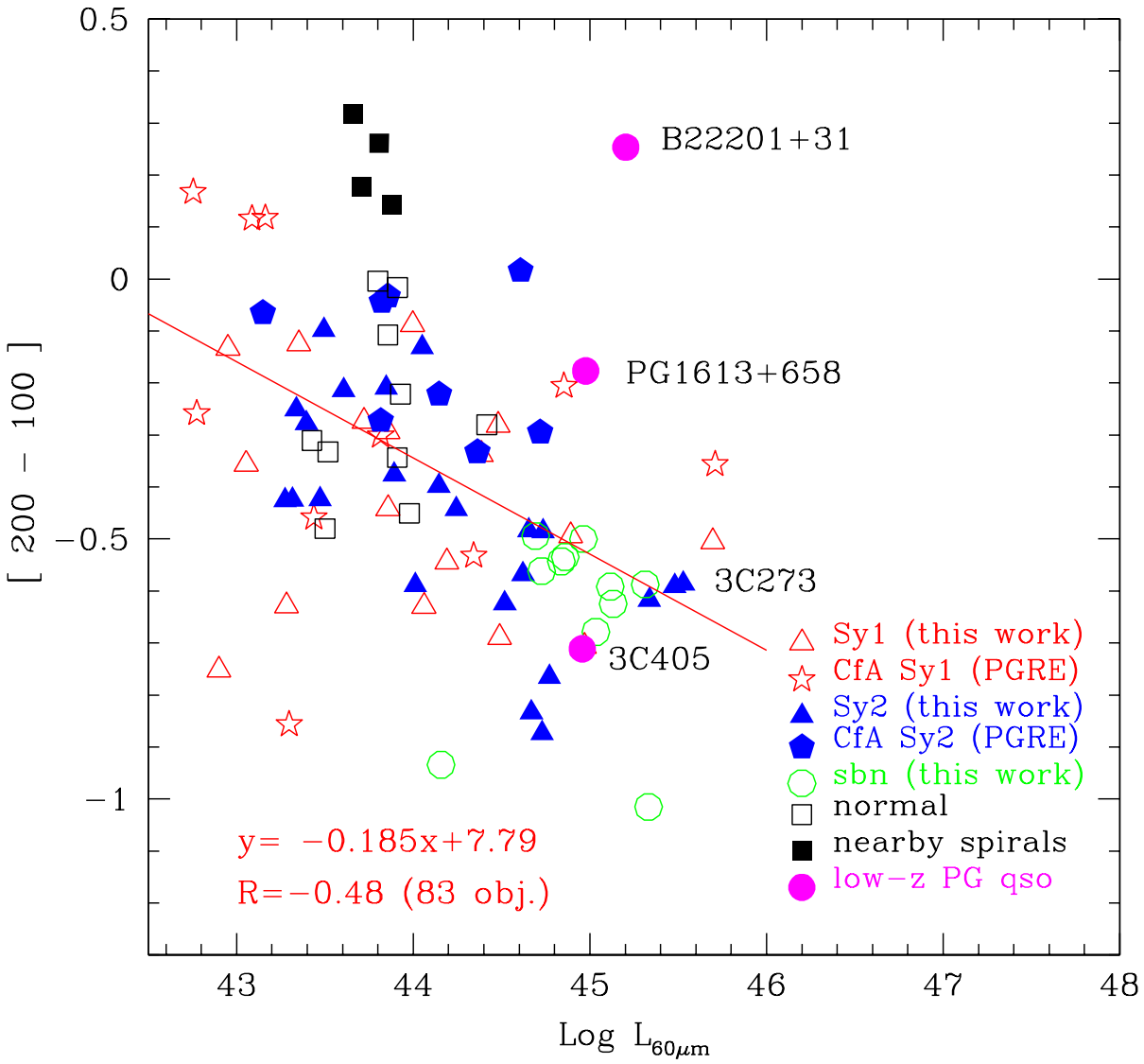

Fig. 18.— The [200 - 100] color versus the 60μm luminosity diagram of galaxies belonging to the 12μm galaxy sample. For comparison are also shown two low redshift (z $\leq$ 0.2) PG quasars and 3C405 (Haas et al. 2000). The solid line represents the linear fit that excludes the 3C objects and the PG quasars, showing a mild correlation between color and 60μm luminosity (the regression coefficient is R=-0.477 for 83 data points).

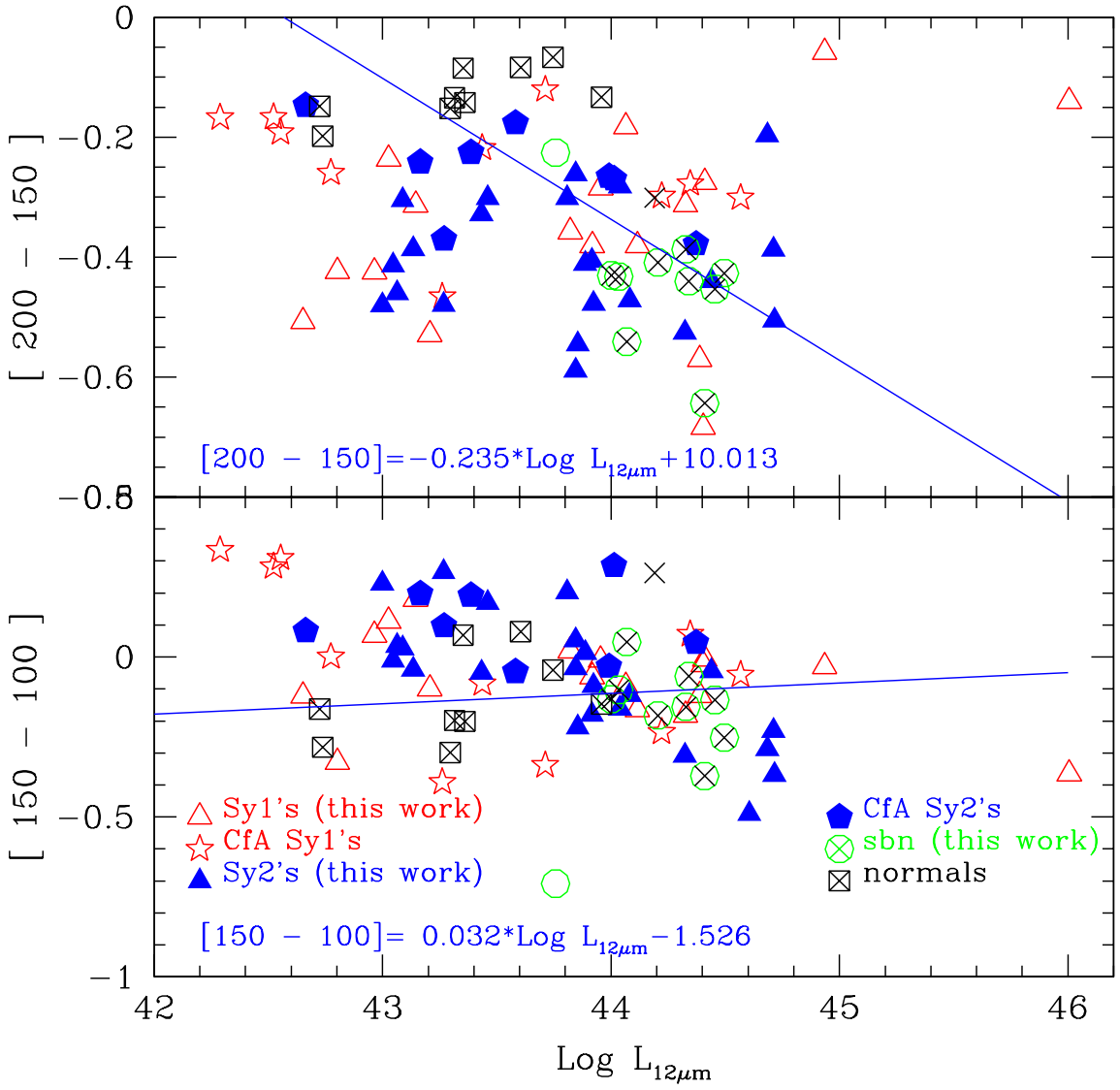

Fig. 19.— Intermediate colors [200 - 150] and [150 - 100] versus 12μm luminosity. The solid line represents the linear fit of the non-Seyfert galaxies (symbols marked with a cross).

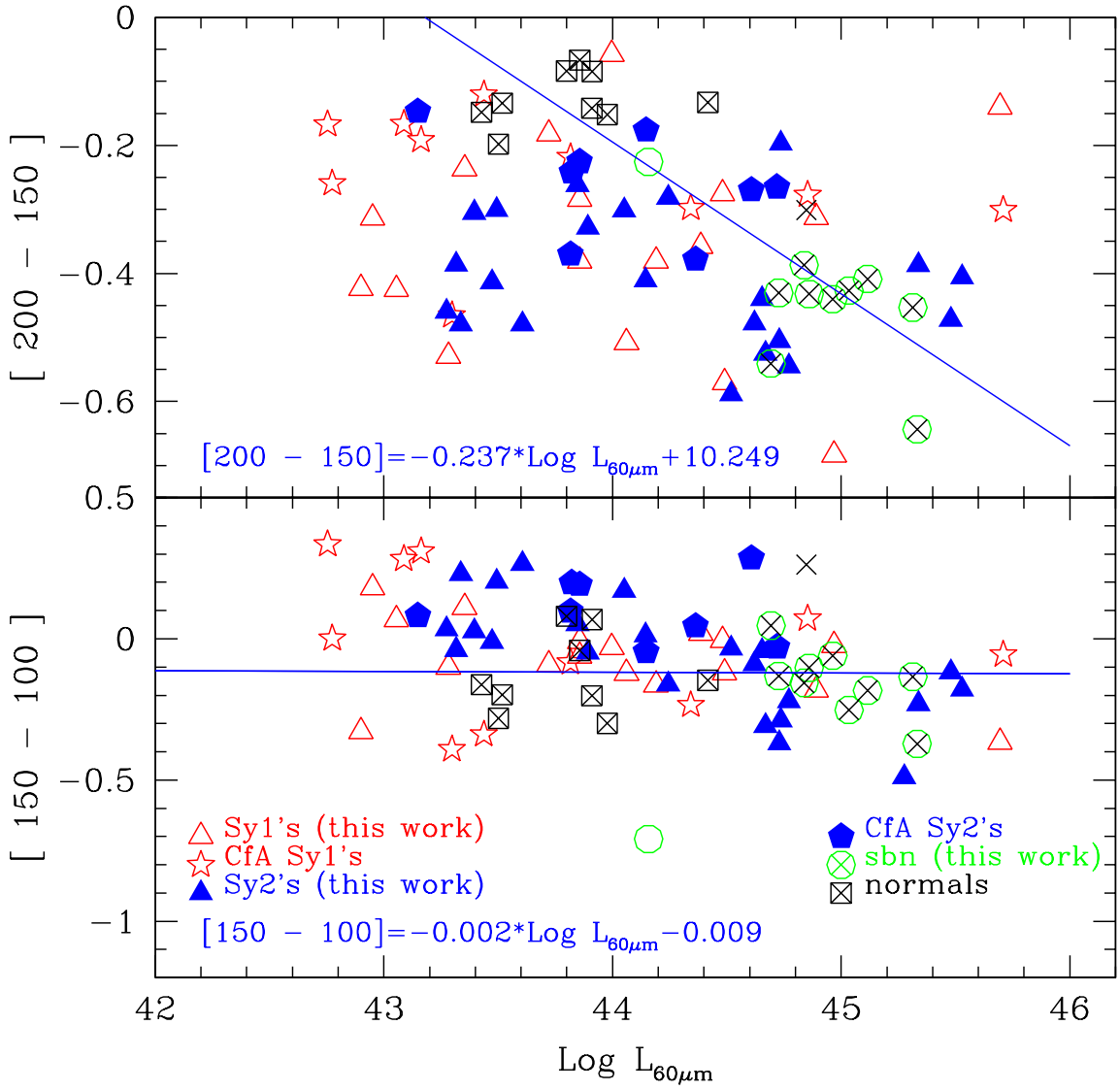

Fig. 20.— Intermediate colors [200 - 150] and [150 - 100] versus 60μm luminosity. The solid line represents the linear fit of the non-Seyfert galaxies (symbols marked with a cross).

Table 1. Journal of the ISOPHOT photometric observations of 12μm active galaxies

Name	R.A.(J2000.0) h m s	Dec.(J2000.0) deg ' "	z	type[a]	Obs.id. (TDT No.)	Time (sec)	ref.
E12-G21	0:40:47.3	-79:14:20.0	0.0328	sy1	55304297	1028	(1)
IZW1	0:53:37.0	12:40:11.8	0.0604	sy1	39502078	992	(2)
MK1034	2:23:20.2	32:11:33.4	0.0380	sy1	65600799	888	(1)
N931=MK1040	2:28:14.4	31:18:42.1	0.0164	sy1	65600803	1380	(1)
NGC1365	3:33:36.5	-36:08:23.1	0.0055	sy1	80301415	230	(1)
F03450+0055	3:47:40.2	1:05:13.8	0.0310	sy1	79501331	974	(2)
MK618	4:36:23.2	-10:22:30.5	0.0347	sy1	67901154	1302	(1)
M-5-13-17	5:19:36.6	-32:39:27.3	0.0125	sy1	67802257	1062	(1)
MK9	7:36:58.6	58:46:12.9	0.0399	sy1	70501363	824	(1)
MK79	7:42:32.0	49:48:35.9	0.0221	sy1	70501666	818	(1)
3C273	12:29:04.4	2:01:45.1	0.1579	sy1/qso	24100607	928	(2)
N4593	12:39:39.4	-05:20:39.3	0.0083	sy1	24600427	424	(2)
M-6-30-15	13:35:50.6	-34:19:07.8	0.0077	sy1	25600791	616	(2)
F13349+2438	13:37:15.0	24:21:47.9	0.1070	sy1	58000935	214	(2)
I4329A	13:49:16.9	-30:20:00.2	0.0161	sy1	25702639	552	(2)
F15091-2107	15:11:58.0	-21:20:28.6	0.0446	sy1	64400729	1082	(2)
N7213	22:09:15.9	-47:09:53.5	0.0059	sy1	35401563	422	(2)
3C445	22:23:47.5	-2:04:48.2	0.0562	sy1	18701453	552	(2)
N7314	22:35:45.8	-26:02:59.9	0.0048	sy1	53905190	448	(1)
MK938	0:11:06.6	-12:06:26.7	0.0192	sy2	55903371	444	(1)
N262=MK348	0:48:47.1	31:57:25.0	0.0151	sy2	59900759	2070	(1)
F00521-7054	0:53:56.2	-70:38:03.4	0.0700	sy2	54201225	578	(1)
M-2-8-39	3:00:30.4	-11:24:56.1	0.0301	sy2	81201040	1784	(1)
N1241	3:11:16.2	-8:55:12.0	0.0072	sy2	79601744	506	(1)
N1320=MK607	3:24:48.7	-3:02:31.7	0.0099	sy2	79501745	870	(1)
F03362-1642	3:38:33.3	-16:32:16.9	0.0360	sy2	79601192	1512	(1)
N1667	4:48:37.6	-6:19:11.8	0.0153	sy2	82203176	464	(1)
F05189-2524	5:21:01.4	-25:21:45.0	0.0415	sy2	86301930	196	(2)
E253-G3	5:25:18.0	-46:00:19.7	0.0407	sy2	72501678	790	(1)
N4501	12:31:59.5	14:25:16.8	0.0077	sy2	23902627/23902607	474/142	(1)
TOL1238-364	12:40:56.9	-36:44:06.7	0.0109	sy2	07800505	516	(2)
N4922A/B	13:01:25.1	29:18:42.2	0.0237	sy2	24500532/24500513	474/392	(1)
M-3-34-64	13:22:24.4	-16:43:42.2	0.0172	sy2	25701422	1124	(1)
MK273	13:44:42.1	55:53:12.8	0.0373	sy2	14201730	180	(2)
MK463	13:56:02.7	18:22:19.0	0.0505	sy2	58001035	196	(2)
ARP220	15:34:57.5	23:30:17.5	0.0182	sy2/ulirg	47600416	750	(2)
F19254-7245	19:31:21.3	-72:39:19.9	0.0615	sy2	10100205	180	(2)
N6810	19:43:33.9	-58:39:20.7	0.0066	sy2	29901651/29901642	474/160	(1)
N6890	20:18:18.1	-44:48:24.5	0.0081	sy2	33602245	1762	(1)
I5063	20:52:02.8	-57:04:13.5	0.0113	sy2	33301248	1124	(1)
N7130=I5135	21:48:19.4	-34:57:03.2	0.0162	sy2	53904967	570	(1)
N7172	22:02:02.1	-31:52:08.8	0.0086	sy2	53905081	460	(1)
F22017+0319	22:04:19.2	3:33:50.2	0.0660	sy2	54000168	2488	(1)
N7496	23:09:46.5	-43:25:43.1	0.0055	sy2	54201073	586	(1)
N7590	23:18:55.2	-42:14:16.9	0.0050	sy2	54200878	562	(1)
N7674=MK533	23:27:56.7	8:46:44.7	0.0290	sy2	55800996	834	(1)
MK551	0:29:25.1	30:33:33.8	0.0500	sbn	58302885	1574	(1)
N232	0:42:45.8	-23:33:37.2	0.0222	sbn	57001381	450	(1)

Table 1—Continued

Name	R.A.(J2000.0) h m s	Dec.(J2000.0) deg ' "	z	type[a]	Obs.id. (TDT No.)	Time (sec)	ref.
IC1623	1:07:46.4	-17:30:26.7	0.0201	sbn	57001288	376	(1)
N838	2:09:38.4	-10:08:48.0	0.0128	sbn	80600207	244	(1)
U2369	2:54:01.7	14:58:15.1	0.0307	sbn	79300510	982	(1)
M+1-33-36	13:01:49.9	4:20:01.5	0.0375	sbn	62000121	644	(1)
IZW107	15:18:06.3	42:44:36.5	0.0400	sbn	57100715	610	(1)
MK496=N6090	16:11:40.7	52:27:29.3	0.0291	sbn	54100719	886	(1)
N6240	16:52:58.8	2:24:09.6	0.0243	sbn	47600512	752	(2)
U11284	18:33:37.2	59:53:22.2	0.0286	sbn	25103948	419	(1)
F20193-2013	20:22:15.4	-20:04:03.3	0.0645	sbn	54200426	1370	(1)
E286-IG19	20:58:26.6	-42:38:57.3	0.0427	sbn	13500535	180	(2)
E148-IG02	23:15:46.8	-59:03:14.6	0.0446	sbn	13501750	180	(2)

Note. — (1): observations belonging to the ISO Open Time Program "IR energy distributions and imaging of the complete sample of $12\mu m$ active galaxies"; (2): ISO archive data.

[a]The galaxy type is coded as follows: sy1: Seyfert 1; sy2: Seyfert 2; sbn: starburst nucleus; ulirg: ultraluminous infrared galaxy.

Table 2. Measured fluxes from ISOPHT C-200 obsrvations of 12μm active galaxies, with 1σ uncertainties.

Name	type	F(120μm) (Jy)	F(150μm) (Jy)	F(170μm) (Jy)	F(180μm) (Jy)	F(200 μm) (Jy)
E12-G21	sy1	···	2.21 ± 0.07	1.81 ± 0.06	1.14 ± 0.02	0.92 ± 0.03
IZW1	sy1	2.57± 0.07	1.89 ± 0.06	1.60 ± 0.05	1.16± 0.07	0.92 ± 0.05
MK1034	sy1	···	10.9 ± 0.1	···	5.68 ± 0.05	2.26 ± 0.10
N931=MK1040	sy1	···	5.54 ± 0.13	5.25 ±0.07	3.72 ± 0.08	2.88 ± 0.03
N1365	sy1	217. ± 0.8	194.0± 0.4	167.0 ± 0.6	103.0± 0.4	85.2 ± 0.5
F03450+0055	sy1	···	1.03 ± 0.19	···	···	0.68 ± 0.15
MK618	sy1	3.32 ± 0.17	3.16 ± 1.50	···	1.19 ± 0.07	0.85 ± 0.04
M-5-13-17	sy1	2.54 ± 0.05	1.86 ± 0.09	···	0.86 ± 0.05	0.55 ± 0.03
MK9	sy1	···	0.74 ± 0.11	···	0.36 ± 0.04	0.23 ± 0.04
MK79	sy1	2.74 ± 0.12	2.04 ± 0.27	1.88 ± 0.15	1.12 ± 0.07	0.85 ± 0.04
3C273	sy1/qso	1.49± 0.13	1.09 ± 0.08	1.10 ± 0.05	0.80± 0.11	0.79 ± 0.11
N4593	sy1	···	8.1 ± 0.1	···	···	4.7 ± 0.1
M-6-30-15	sy1	···	1.06 ± 0.04	···	···	0.40 ± 0.06
F13349+2438	sy1	···	···	0.35 ± 0.02	···	···
I4329A	sy1	···	1.87± 0.08	···	···	1.2 ± 0.2
F15091-2107	sy1	···	1.47± 0.03	···	···	0.78 ± 0.07
N7213	sy1	···	13.62±0.35	···	···	6.6 ± 0.4
3C445	sy1	···	0.56± 0.08	···	···	0.49 ± 0.16
N7314	sy1	24.5 ± 0.5	19.4 ± 0.4	17.4 ± 0.3	11.3 ± 0.2	7.3 ± 0.2
MK938=N34	sy2	17.2 ± 0.4	10.6 ±0.5	8.5±0.2	5.4±0.1	3.0±0.1
N262=MK348	sy2	2.24 ± 0.08	2.28 ±0.04	1.89±0.03	1.29±0.02	1.14±0.04
F00521-7054	sy2	···	0.22±0.02	···	0.087±0.017	···
M-2-8-39	sy2	1.46 ± 0.05	1.26 ±0.03	···	0.762±0.015	···
N1241	sy2	17.6 ± 0.6	18.2 ±3.6	14.6±2.6	8.12±0.10	6.03±0.09
N1320=MK607	sy2	3.7 ± 0.1	2.58 ±0.36	···	1.44±0.05	1.06±0.04
F03362-1642	sy2	1.55 ± 0.14	0.59 ±0.08	···	0.39±0.03	0.39±0.03
N1667	sy2	29.6 ± 8.8	16.3 ±0.5	17.0±2.8	9.03±0.15	6.33±0.17
F05189-2524	sy2	10.6 ± 0.4	7.0 ±0.4	···	3.2±0.3	2.9±0.4
E253-G3	sy2	2.74 ± 0.17	1.71 ±0.19	···	0.86±0.14	0.51±0.04
N4501	sy2	116 ± 0.3	94.1 ±0.9	···	52.3±0.4	47.0±0.5
TOL1238-364	sy2	···	···	7.42±0.11	4.60±0.06	3.62±0.11
N4922A/B	sy2	6.8±0.9	7.1 ±1.8	···	2.97±0.03	1.83±0.08
M-3-34-64	sy2	6.4±0.3	4.4 ±0.4	···	3.6±0.2	2.3±0.4
MK273	sy2	23.6±0.52	16.95±0.22	···	7.48±0.20	5.75±0.30
MK463	sy2	2.26±0.40	0.80±0.15	···	< 0.30	< 0.25
ARP220	sy2/ulirg	117.3±0.2	79.4±0.2	71.4±0.1	41.1±0.1	31.2±0.3
F19254-7245	sy2	3.5±0.5	2.6±0.3	···	0.7±0.2	···
N6810	sy2	···	29.8±0.1	···	16.9±0.2	14.0±0.2
N6890	sy2	11.7±0.1	8.8±0.1	···	5.09±0.03	4.36±0.05
I5063	sy2	4.97±0.35	4.13±0.35	···	3.10±0.26	2.26±0.38
N7130=IC5135	sy2	28.9±1.7	21.9±3.0	16.9±1.0	10.8±0.6	7.29±0.47
N7172	sy2	32.0±9.2	22.9±4.7	19.0±3.2	12.6±0.4	7.60±0.43
F22017+0319	sy2	···	0.85±0.13	···	···	0.54±0.02
N7496	sy2	20.8±0.1	16.2±0.2	13.9±0.5	8.89±0.12	6.25±0.07
N7590	sy2	25.9±0.1	22.8±2.7	17.6±0.2	12.4±0.8	7.91±0.08
N7674=MK533	sy2	9.38±0.18	7.65±0.37	6.02±0.06	3.67±0.11	2.78±0.04
MK551	sbn	5.11±0.10	3.42±0.10	···	1.68±0.03	1.28±0.03
N232	sbn	18.1±0.4	18.9±5.2	15.7±3.9	9.11±1.5	5.44±0.09

Table 2—Continued

Name	type	F(120μm) (Jy)	F(150μm) (Jy)	F(170μm) (Jy)	F(180μm) (Jy)	F(200 μm) (Jy)
IC1623	sbn	36.5±0.3	26.7±0.3	23.5±0.4	12.80±0.07	9.69±0.09
N838	sbn	···	4.07±0.13	···	2.84±0.08	2.42±0.14
U2369	sbn	11.1±0.1	8.71±0.22	6.97±0.09	4.27±0.07	3.22±0.10
M+1-33-36	sbn	7.25±0.06	5.90±0.08	6.48±1.50	3.45±0.04	2.42±0.05
IZW107	sbn	9.84±0.09	11.3±4.7[a]	9.0±3.8[a]	3.18±0.04	2.29±0.08
MK496=N6090	sbn	9.98±0.10	6.87±0.10	···	3.47±0.03	2.55±0.04
N6240	sbn	23.7±0.3	18.2±0.2	16.7±0.1	9.5±0.1	7.1±0.3
U11284	sbn	35.1±0.3	27.0±0.2	···	14.5±0.2	13.5±0.3
F20193-2013	sbn	3.98±0.04	3.00±0.05	···	1.26±0.02	···
E286-IG19	sbn	7.0± 0.3	4.4± 0.2	···	2.1±0.1	1.0±0.3
E148-IG02	sbn	11.4±0.6	7.95±0.25	···	4.31±0.18	2.8±0.3

[a]The low value of the signal to noise is due to a large uncertainty in the internal calibrator measurements.

Table 3. Total integrated mid- to far-infrared luminosities of 12μm active galaxies

Name	Log(L_{FIR}) (erg s^{-1})	type	Name	Log(L_{FIR}) (erg s^{-1})	type	Name	Log(L_{FIR}) (erg s^{-1})	type
E12-G21	44.501	sy1	N262=MK348	43.966	sy2	N7496	43.808	sy2
IZW1	45.303	sy1	F00521-7054	45.005	sy2	N7590	43.718	sy2
MK1034	45.147	sy1	N1068[a]	44.763	sy2	N7582[b]	44.416	sy2
N931=MK1040	44.320	sy1	N1143/4[a]	45.145	sy2	N7674=MK533	45.040	sy2
N1365	44.815	sy1	M-2-8-39	44.221	sy2	MK551	45.229	sbn
F03450+0055	44.192	sy1	N1241	43.922	sy2	N232	45.035	sbn
MK618	44.802	sy1	N1320=MK607	43.691	sy2	I1623	45.221	sbn
M-5-13-17	43.705	sy1	F03362-1642	44.422	sy2	N838	44.328	sbn
MK9	44.452	sy1	N1667	44.696	sy2	U2369	45.114	sbn
MK79	44.313	sy1	F05189-2524	45.498	sy2	M+1-33-36	45.111	sbn
N3227[a]	43.640	sy1	E253-G3	44.900	sy2	IZW107	45.377	sbn
N3516[a]	43.588	sy1	N3079[a]	44.256	sy2	MK496=N6090	44.958	sbn
N4051[a]	43.350	sy1	N3982[a]	43.602	sy2	N6240	45.308	sbn
N4151[a]	43.317	sy1	N4388[a]	44.315	sy2	F20193-2013	45.097	sbn
MK766=N4253[a]	44.098	sy1	N4501	44.637	sy2	E286-IG19	45.387	sbn
3C273	46.071	sy1	TOL1238-364	44.149	sy2	E148-IG02	45.450	sbn
N4593	43.640	sy1	N4922A/B	44.715	sy2	N245=MK555[c]	44.037	nor
MK231[a]	45.930	sy1	M-3-34-64	44.532	sy2	U2936[c]	44.357	nor
N5033[a]	43.811	sy1	N5256=MK266[a]	44.983	sy2	U2982[c]	44.696	nor
M-6-30-15	43.219	sy1	MK273	45.572	sy2	N5430=MK799[c]	44.194	nor
F13349+2438	45.508	sy1	MK463	45.102	sy2	N5719[c]	43.692	nor
I4329A	44.240	sy1	N5929[a]	44.128	sy2	N6918[c]	43.684	nor
N5548[a]	43.930	sy1	ARP220	45.669	sy2	N7083[c]	44.398	nor
MK817[a]	44.619	sy1	F19254-7245	45.415	sy2	N7624=MK323[c]	44.234	nor
F15091-2107	44.693	sy1	N6810	44.125	sy2	N7714=MK538[c]	44.111	nor
N7213	43.466	sy1	N6890	43.815	sy2	N7798=MK332[c]	43.781	nor
3C445	44.540	sy1	I5063	44.182	sy2	N134[d]	44.034	nea
N7314	43.650	sy1	N7130=IC5135	44.916	sy2	N660[d]	43.809	nea
N7469[a]	45.131	sy1	N7172	44.239	sy2	N5194=M51[d]	44.100	nea
MK938=N34	44.923	sy2	F22017+0319	45.013	sy2	N5236=M83[d]	44.127	nea

[a]ISOPHOT data from Pérez García & Rodríguez Espinosa (2000)

[b]ISOPHOT data from Radovich et al. (1999)

[c]ISOPHOT data from Siebenmorgen, Krugel & Chini (1999)

[d]ISOPHOT data from Alton et al. (1998)

Note. — The galaxy type is coded as follows: sy1: Seyfert 1; sy2: Seyfert 2; sbn: starburst nucleus; nor: normal galaxy; nea: nearby spiral galaxy.

Table 4. Averaged colors with 1σ uncertainties and spectral indices for the various classes of galaxies belonging to the 12μm galaxy sample .

Galaxy class	[60 - 25]	[100 - 60]	[200 - 100]	$\alpha_{25-60\mu m}$	$\alpha_{60-100\mu m}$	$\alpha_{100-200\mu m}$	$\alpha_{12-100\mu m}$
Seyfert 1's	0.40±0.30	0.23±0.15	-0.43±0.21	-1.1	-1.0	1.4	-1.0
CfA Seyfert 1's	0.47±0.29	0.19±0.17	-0.26±0.32	···	···	···	···
Seyfert 2's	0.62±0.29	0.16±0.18	-0.47±0.21	-1.6	-0.7	1.6	-1.4
CfA Seyfert 2's	0.77±0.26	0.23±0.09	-0.16±0.14	···	···	···	···
Starburst	0.82±0.16	0.11±0.09	-0.66±0.21	-2.1	-0.5	2.2	-1.7
Normal galaxies	0.84±0.12	0.28±0.12	-0.25±0.17	-2.2	-1.3	0.8	-1.6
Nearby spirals	0.83±0.10	0.39±0.15	0.22±0.08	-2.2	-1.7	-0.7	-1.6

Table 5. Measured fluxes from ISOPHT C-100 observations of 12μm active galaxies, with 1σ statistical uncertainty.

Name	F(60μm) (Jy)	F(65μm) (Jy)	F(80μm) (Jy)	F(90μm) (Jy)	F(100μm) (Jy)	F(105μm) (Jy)	notes
F00521-7054	1.26±0.04	1.10±0.08	1.10±0.04	0.63±0.03	···	0.83±0.04	
N7674	3.5±0.1	4.6±0.1	4.0±0.1	2.99±0.06	···	3.7±0.1	
F03362-1642	1.10±0.05	···	1.10±0.04	1.01±0.03	···	1.10±0.04	
M+1-33-36	5.5±1.0	···	5.7±1.0	···	7.8±1.0	5.2±1.0	(1)
N262	0.74±0.07	0.67±0.07	0.87±0.05	0.73±0.03	0.93±0.04	···	(1)
N1365	81.9±1.0	121.0±1.0	···	114.0±1.0	···	···	
N4501	18.0±0.2	···	···	35.0±0.4	···	···	(1)
N4922AB	5.20±0.1	···	···	6.10±0.1	···	···	
N6890	8.4±0.6	···	···	15.8±0.9	···	···	

Note. — (1): extended emission detected